The multi PAM2 protein Upa2 functions as novel core component of endosomal mRNA transport

Silke Jankowski[1,†], Thomas Pohlmann[1, †], Sebastian Baumann[1, #], Sabrina Zander[1], Senthil Kumar Devan[1] and Michael Feldbrügge[1, *]

[†] equal contribution

[1] Heinrich Heine University Düsseldorf, Institute for Microbiology, Cluster of Excellence on Plant Sciences, 40204 Düsseldorf, Germany

present address: Cell and Developmental Biology, Centre for Genomic Regulation (CRG), Barcelona, Spain

Running title: An atypical Pab1 interactor for endosomal mRNA transport

Word count: 4507

Key words: endosome / microtubule / MLLE domain / PAM2 motif / poly(A)-binding protein / RNA transport

[*] Corresponding author:

Dr. Michael Feldbrügge

Institute for Microbiology, Cluster of Excellence on Plant Sciences

Heinrich Heine University Düsseldorf; 40204 Düsseldorf, Germany,

Phone: +49 (211) 81-15475,

feldbrue@hhu.de

Abstract

mRNA transport determines spatiotemporal protein expression. Transport units are higher-order ribonucleoprotein complexes containing cargo mRNAs, RNA-binding proteins and accessory proteins. Endosomal mRNA transport in fungal hyphae belongs to the best-studied translocation mechanisms. Although several factors are known, additional core components are missing. Here, we describe the 232 kDa protein Upa2 containing multiple PAM2 motifs (poly[A]-binding protein [Pab1] associated motif 2) as a novel core component. Loss of Upa2 disturbs transport of cargo mRNAs and associated Pab1. Upa2 is present on almost all transport endosomes in an mRNA dependent-manner. Surprisingly, all four PAM2 motifs are dispensable for function during unipolar hyphal growth. Instead, Upa2 harbours a novel N-terminal effector domain as important functional determinant as well as a C-terminal GWW motif for specific endosomal localisation. In essence, Upa2 meets all the criteria of a novel core component of endosomal mRNA transport and appears to carry out crucial scaffolding functions.

15 **Introduction**

16 Active transport of mRNAs determines when and where proteins are synthesised. Such
17 trafficking events are important for a wide variety of different cellular processes like
18 asymmetric cell division, polar growth, embryonic development and neuronal activity
19 (Eliscovich & Singer, 2017, Martin & Ephrussi, 2009). Several mRNA translocation
20 mechanisms have been described. During cytokinesis of *Saccharomyces cerevisiae*, for
21 example, the actin-dependent transport of *ASH1* mRNA is mediated by the concerted binding
22 of the RNA-binding proteins (RBP) She2p and She3p. These RBPs connect the cargo mRNA
23 to the myosin motor Myo4 for transport towards the daughter cell (Edelmann et al., 2017,
24 Niessing et al., 2018). In highly polarised cells such as fungal hyphae and neurons, mRNAs are
25 transported along microtubules over long distances. Here, molecular motors such as kinesins
26 and dynein are involved. Among the best studied examples of microtubule-dependent
27 translocation is the mRNA transport on shuttling endosomes during polar hyphal growth in the
28 fungus *Ustilago maydis* (Mofatteh & Bullock, 2017).

29 Upon infection of corn, *U. maydis* switches from budding to hyphal growth (Haag et al.,
30 2015, Vollmeister et al., 2012). The resulting infectious hyphae grow with a defined axis of
31 polarity: they expand at the apical pole and insert septa at the basal pole resulting in the
32 formation of characteristic sections devoid of cytoplasm. In this growth mode, hyphae depend
33 on active transport along microtubules. Loss of long-distance transport results in aberrant
34 hyphal growth. Characteristic of this defect is the formation of bipolarly growing cells.
35 Important carriers are Rab5a-positive endosomes that shuttle along microtubules by the
36 concerted action of the plus-end directed Kinesin-3 type motor Kin3 and the minus-end directed
37 cytoplasmic dynein Dyn1/2 (Baumann et al., 2012, Schuster et al., 2011). These endosomes
38 carry characteristic markers of early endosomes involved in endocytosis (Haag et al., 2017).
39 However, during polar growth they also function as transport endosomes moving organelles,

40 like peroxisomes, and mRNAs with associated ribosomes attached to their cytoplasmic surface
41 (Baumann et al., 2014, Higuchi et al., 2014).

42 The key RNA-binding protein for mRNA transport is Rrm4, an RRM (RNA recognition
43 motif) protein containing tandem N-terminal RRMs separated by a spacer from a third RRM
44 domain (Figure 1A). The mRNAs of all four septins were identified to be important cargo
45 mRNAs, which are most likely translationally active while being transported on endosomes
46 (Baumann et al., 2014, König et al., 2009, Zander et al., 2016). Consequently, the translation
47 products Cdc3, Cdc10, Cdc11 and Cdc12 form heteromeric complexes on the cytoplasmic
48 surface of endosomes in an Rrm4-dependent manner. These septin complexes are delivered to
49 the hyphal growth pole to form a longitudinal gradient of filaments (Baumann et al., 2014,
50 Zander et al., 2016). A recent transcriptome-wide view of endosomal mRNA transport revealed
51 that Rrm4 binds thousands of mRNAs preferentially in their 3′ UTR in close proximity to the
52 small glycine rich protein Grp1. This extensive mRNA transport is most likely needed for the
53 distribution of mRNAs within the fast-growing hypha as well as for the transport of specific
54 mRNAs encoding e.g. septins for heterooligomerisation (Olgeiser et al. *in revision*).

55 At its C-terminus, Rrm4 carries two MademoiseLLE (MLLE) domains that function as
56 peptide binding pockets for specific interaction with the PAM2-like motifs of Upa1. Upa1 links
57 Rrm4-containing mRNPs to transport endosomes using a FYVE zinc finger domain to
58 recognise phosphatidylinositol-3-phosphate lipids of early endosomes. (Pohlmann et al., 2015).
59 In addition, Upa1 also carries a classical PAM2 motif for interaction with the MLLE domain
60 of the poly(A)-binding protein Pab1, an additional component of endosomal mRNPs (Becht et
61 al., 2006, Haag et al., 2015). Although we already identified a number of components of
62 endosomal mRNA transport, key factors might still be missing. Here, we unravelled and
63 characterized one such factor, the protein Upa2, a second *Ustilago* PAM2 motif protein that
64 had previously been identified by bioinformatic prediction of PAM2-containing proteins
65 (Pohlmann et al., 2015).

66 **Results**

67 **The PAM2-containing protein Upa2 interacts with Pab1**

68 Upa2 (*Ustilago* PAM2 protein 2; UMAG_10350) is a 2121 amino acid (aa) protein with a
69 conserved coiled coil domain of unknown function at its C-terminus, as well as four PAM2
70 motifs for potential interaction with the MLLE domain of Pab1. One PAM2 motif is situated at
71 the immediate N-terminus and three in the central region of the protein (Figure 1A-B).

72 In order to validate the predicted PAM2 motifs we performed yeast two-hybrid studies that
73 have already been successfully applied to demonstrate an interaction between Pab1 and the
74 PAM2 motif of Upa1 (Pohlmann et al., 2015). Full-length Upa2 shows weak interaction with
75 Pab1 but did not interact with Rrm4 (Figure 1C, Supplementary Figure S1A). The latter is
76 consistent with the observation that PAM2-like motifs for Rrm4 interaction are missing in Upa2
77 (Pohlmann et al., 2015). Upon mapping the interaction domain of Upa2 with Pab1 we observed
78 that the PAM2-containing N-terminal part of Upa2 (aa 1-1216) but not the C-terminal part (aa
79 1217-2121) interacted with Pab1 (Figure 1C). The interaction of Upa2 with Pab1 was mediated
80 by the MLLE domain of Pab1, since this domain was necessary and sufficient for reporter gene
81 expression in the yeast two-hybrid system (Figure 1C, Supplementary Figure S1A). Mutational
82 analysis of the PAM2 motifs in Upa2 revealed that a single PAM2 motif was sufficient for
83 interaction with the MLLE domain of Pab1 or full length Pab1 (Supplementary Figure S1A).
84 Mutating all PAM2 motifs resulted in loss of interaction of Upa2 with the MLLE domain of
85 Pab1 (Figure 1C) and strongly reduced interaction with Upa2 and full length Pab1
86 (Supplementary Figure S1A).

87 To verify this binding behaviour, we tested the interaction of the central PAM2 triplet of
88 Upa2 (aa 834-1216) with the MLLE domains of Pab1 by GST-pulldown experiments using
89 variants expressed in *Escherichia coli*. These experiments confirmed the specific interaction of
90 the PAM2 motifs of Upa2 with the MLLE domain of Pab1. The interaction strength was

91 dependent on the number of functional PAM2 motifs (Figure 1D). As expected, PAM2 motifs
92 of Upa2 did not interact with Rrm4 (Supplementary Figure S1B-C).
93 Since coiled coil domains have been described as dimerization regions, we tested this in a
94 yeast two-hybrid assay. When appended to both BD and AD reporter proteins the predicted C-
95 terminal coiled coil domain of Upa2 supported yeast growth on selective medium suggesting
96 that this region indeed functions as a dimerization domain (Figure 1E). Taken together, Upa2
97 contains multiple functional PAM2 motifs for interaction with Pab1 and a C-terminal
98 dimerization domain. The interaction with Pab1 is the first hind that Upa2 might function in
99 endosomal mRNA transport.

100 **Upa2 is essential for efficient unipolar hyphal growth**

101 If Upa2 is indeed important for endosomal mRNA transport, loss of Upa2 should exhibit
102 phenotypes similar to mutations in the previously identified transport components Rrm4 and
103 Upa1 (Pohlmann et al., 2015). To test this assumption, we generated *upa2* deletion mutants in
104 the genetic background of laboratory strain AB33. In this strain, hyphal growth can be elicited
105 synchronously and reproducibly by switching the nitrogen source in the medium (Brachmann
106 et al., 2001). Hyphae grow with a defined axis of polarity: they expand at the apical tip and
107 insert septa at their base leading to the formation of characteristic empty sections (Figure 2A).
108 While loss of Upa2 did not affect growth or alter shape of yeast cells (Supplementary Figure
109 S2A-B) *upa2*Δ strains exhibited a bipolar growth phenotype and the formation of empty
110 sections was delayed. This aberrant growth mode is typical for defects in microtubule-
111 dependent transport and has been described for loss of the key proteins of endosomal mRNA
112 transport like Rrm4 and Upa1 (Figure 2A-B). Analysing the *upa1*Δ/*upa2*Δ double mutant
113 revealed that the number of hyphae exhibiting aberrant bipolar hyphal growth was not additive
114 (Supplementary Figure S2), providing genetic evidence that both PAM2-containing proteins
115 function in the same cellular process.

116 A second read-out for defects in the endosomal mRNA transport machinery is the
117 unconventional secretion of chitinase Cts1 (Koepke et al., 2011, Pohlmann et al., 2015). Loss
118 of Upa2 resulted in reduced extracellular Cts1 activity specifically during hyphal growth. This
119 is reminiscent of defective Cts1 secretion upon deletion of *rrm4* and *upa1* (Supplementary
120 Figure S2D). Hence, Upa2 might function in concert with Rrm4 and Upa1 during endosomal
121 mRNA transport.

122 This hypothesis was supported by a phylogenetic analysis showing that orthologs of Upa2
123 were found in several basidiomycete fungi with comparable spacing of the predicted PAM2
124 motifs (Figure 2C). Consistent with the notion that Rrm4, Upa1 and Upa2 function together,
125 these fungi also had orthologs for Rrm4 and Upa1. Notably, Upa2 was absent in fungi, which
126 presumably have lost the endosomal mRNA transport machinery, like *Malassezia globosa* and
127 *Cryptococcus neoformans var. neoformans*. The latter only possesses diverged orthologs of
128 Rrm4 and Upa1 lacking key functional domains, while *M. globosa* is even lacking a clear
129 ortholog of Rrm4 (Figure 2C). In essence, the evolutionarily conserved Upa2 is a novel factor
130 essential for efficient unipolar growth that might function in endosomal mRNA transport.

131 **Upa2 shuttles on Rrm4-positive transport endosomes**

132 *upa2* and *rrm4* appear to be genetically and phyogenetically linked. We therefore examined
133 whether the protein can also be found on transport endosomes by expressing a functional
134 version of Upa2 with C-terminally fused Gfp (eGfp, Clontech; Figure 2A-B; Supplementary
135 Figure S2D). Fluorescence microscopy revealed that in hyphae Upa2-Gfp localised exclusively
136 in bidirectionally moving units (Figure 3A, Supplementary Video V1). Movement was
137 inhibited by benomyl indicating that it was microtubule-dependent (Figure 3A, Supplementary
138 Video V1). Importantly, Upa2-Gfp shuttling resembled the movement of Rrm4-Gfp and Pab1-
139 Gfp (Figure 3A, Supplementary Video V1). This holds true for the amount of processive signals

140 as well as for their velocity (Figure 3B-C). Hence, Upa2 appeared to shuttle on Rrm4-positive
141 transport endosomes (Baumann et al., 2012, Pohlmann et al., 2015).

142 For experimental verification of endosomal shuttling we stained processive endosomes
143 with the lipophilic dye FM4-64 (Haag et al., 2017). Using dual-colour dynamic live imaging,
144 we detected extensive co-localisation of Upa2-Gfp and FM4-64-stained, processively moving
145 endosomes (Figure 3D-E). Furthermore, we tested strains co-expressing Upa2-Gfp and Rrm4-
146 mCherry or Pab1-mCherry (functional C-terminal fusions with the monomeric red fluorescent
147 protein mCherry; Baumann et al., 2014, König et al., 2009). In this instant we also observed
148 extensive co-localisation of Upa2 and Rrm4 (Figure 3D-E, Supplementary Video V2)
149 indicating that Upa2 was present on almost all shuttling endosomes (Baumann et al., 2012,
150 Pohlmann et al., 2015). Upa2-Gfp also co-localised with processively moving Pab1-mCherry
151 (Figure 3D-E). However, unlike Rrm4, Pab1-mCherry additionally localised in the cytoplasm
152 resulting in diffuse and static signals that are easily detectable around the region of the nucleus
153 (Figure 3A, D; Baumann et al., 2014, König et al., 2009). Notably, Upa2 did not exhibit this
154 cytoplasmic staining indicating that it is not present in cytoplasmic Pab1-containing complexes,
155 but specifically interacts with endosome-associated Pab1 (Figure 3A, D, E). In essence, Upa2
156 shuttles exclusively on almost all Rrm4-positive transport endosomes supporting the notion that
157 it is a new component of endosomal mRNPs.

158 **Endosomal localisation of Upa2 depends on the RNA-binding capacity of Rrm4**

159 Since Upa2 proved to be an endosomal protein, we investigated the functional relationship
160 between Upa2 and Rrm4 by studying the subcellular localisation of endosomal mRNP
161 components in *rrm4*Δ strains. As previously described, the endosomal localisation of Upa1-Gfp
162 is not affected in *rrm4*Δ strains, because its interaction is mRNA-independent and mediated by
163 its FYVE domain (Figure 4A-B, Supplementary Video V3; Pohlmann et al., 2015). In contrast,
164 Pab1-Gfp is no longer detectable on shuttling endosomes in *rrm4*Δ strains indicating that

165 without Rrm4 no mRNAs are transported on endosomes (Figure 4A-B, Supplementary Video
166 V4; König et al., 2009). Interestingly, the endosomal localisation of Upa2 was also no longer
167 detectable in *rrm4*Δ strains (Figure 4A-B, Supplementary Video V5) suggesting that the
168 association of Upa2 depends on direct interaction with endosomal mRNP components.

169 To investigate a possible mRNA-dependent interaction of Upa2 with shuttling endosomes
170 we studied the effect of the allele Rrm4^{mR1}-Rfp (Rrm4 variant with C-terminally fused
171 monomeric Rfp). Previously, it was shown that Rrm4^{mR1} carrying a loss of function mutation
172 in the first RRM domain resulted in drastically reduced RNA binding of Rrm4 (Becht et al.,
173 2006). Notably, Upa2 is no longer detectable on endosomes in a Rrm4^{mR1}-Rfp background,
174 whereas for Pab1 we observed a strong reduction in movement (Figure 4C-D, Supplementary
175 Videos V6-7). This indicates that the recruitment of Upa2 to motile transport endosomes is
176 dependent on the RNA-binding capacity of Rrm4. Taken together, although loss of the
177 endosomal components Upa1 and Upa2 results in similar defects during hyphal growth, the
178 mode of endosomal localisation is clearly different. Contrary to Upa1, endosomal localisation
179 of Upa2 is mRNA-dependent, suggesting an interaction with mRNA either directly or indirectly
180 through a protein component of mRNPs such as Pab1 that Upa2 binds via its PAM2 motifs.

181 **Upa2 carries two functionally important regions, a N-terminal effector domain and a C-**
182 **terminal GWW motif**

183 Since the mRNA-dependent localisation could be explained by the direct PAM2-dependent
184 interaction with Pab1, we tested the role of the identified PAM2 motifs of Upa2 with regards
185 to function and endosomal localisation. Therefore, we expressed Upa2-Gfp variants in
186 laboratory strain AB33 carrying mutations in one, in multiple and in all identified PAM2 motifs.
187 Surprisingly, none of the PAM2 mutations affected the hyphal growth of *U. maydis* indicating
188 that the interaction of Upa2 with Pab1 is not essential for its role during hyphal growth (Figure
189 5A-B). Furthermore, endosomal shuttling was not affected by mutating all four PAM2s
190 indicating that the interaction with Pab1 is dispensable for endosomal localisation

191 (Supplementary Figure S3A). Hence, Upa2 must contain so far unknown domains critical for
192 endosomal transport functions.

193 To map these domains, we studied N-terminal truncations carrying C-terminal Gfp fusions
194 (Figure 5C). Respective alleles were integrated at the homologous locus. Removal of the first
195 338 amino acids did not interfere with the function of the protein (Upa2-339-2121; Figure 5C-
196 D). However, additional truncations resulted in increase of bipolar hyphae indicating reduced
197 (Upa2-399-2121) or loss of function (Upa2-599-2121; Figure 5C-D). Importantly, endosomal
198 shuttling of these versions and protein amounts were not drastically affected (Figure 5E;
199 Supplementary Figure 5B). Hence, a currently unknown effector domain important for
200 endosomal mRNA transport is located between amino acid position 339 and 599. Notably, the
201 non-functional variant Upa2-599-2121 still contained three PAM2 motifs, consistent with the
202 finding that the interaction with Pab1 is not sufficient for function.

203 For mapping of the domain that mediates endosomal localisation of Upa2, we assayed
204 additional N-terminal truncations. All variants still shuttled indicating that the last 163 amino
205 acids were sufficient for endosomal shuttling (Figure 5C, F). Upa2-1217-2121 did no longer
206 contain any PAM2 region for interaction with Pab1 (Figure 5C). This was consistent with the
207 finding that the PAM2 motifs of Upa2 were not essential for endosomal localisation. Closer
208 inspection by sequence comparison revealed a conserved GWW sequence at the very C-
209 terminus (Figure 5G), which was shown in other proteins to function in protein/protein
210 interaction (Hardwick et al., 2011, Hardwick et al., 2012). Mutating this short sequence resulted
211 in loss of shuttling without drastic changes in protein amounts (Figure 5F, Supplementary
212 Figure S3B). This holds true when testing the mutation in the context of the full length protein
213 (Figure 5H, Supplementary Video V8). Importantly, we also observed a loss of function
214 phenotype for this mutation, i.e. an increased number of bipolar hyphae (Figure 5H,
215 Supplementary Figure S3C). This was not due to altered protein amounts (Supplementary
216 Figure 3B). Thus, the conserved C-terminal GWW motif is essential for endosomal localisation

217 of Upa2 and endosomal localisation is important for the function of the protein. In essence,
218 besides the PAM2 motifs, Upa2 contains a functionally important N-terminal effector domain
219 and a C-terminal GWW motif for interaction with an endosomal mRNP component (see
220 Discussion).

221 **Loss of Upa2 causes defects in the formation of endosomal mRNPs**

222 Finally, we studied the role of Upa2 during endosomal mRNA transport in closer detail. An
223 important function of endosomal mRNA transport is the local assembly of septin heteromeric
224 subunits that are transported to hyphal growth poles to form filaments with a gradient emanating
225 from this pole (Baumann et al., 2014, Zander et al., 2016). Using a functional septin fusion
226 protein Cdc3-Gfp as read-out (Cdc3 N-terminally fused to eGfp; Baumann et al., 2014) we
227 observed that loss of Upa2 abolished endosomal shuttling of Cdc3-Gfp and as an expected
228 consequence also the Cdc3-Gfp containing gradient at hyphal tips was no longer detectable
229 (Figure 6A-C, Supplementary Video V9).

230 Studying septin mRNA transport with RNA live imaging (Baumann et al., 2015;
231 Supplementary Figure S4A) revealed that the number of processively transported *cdc3B*^{16}
232 mRNAs was reduced to about 50% (Figure 6D-E). While the velocity of the *cdc3B*^{16} containing
233 mRNPs was not affected (Supplementary Figure S4B), the range of movement was reduced
234 (Figure 6F) suggesting that mRNPs might fall off endosomes with higher frequency.

235 To address whether the defect is specific to the *cdc3* mRNA we tested shuttling of other
236 endosomal components. In case of Rrm4-Gfp we observed that Rrm4-Gfp still shuttles in
237 *upa2*Δ strains, although a substantial fraction of the protein also stained structures that
238 resembled microtubule bundles (Figure 6G; Supplementary Figure 4C). Consistently, in
239 benomyl treated hyphae bundle-like Rrm4-Gfp signals were no longer detected (Supplementary
240 Figure S4D-E). This suggests that Rrm4 localisation is disturbed in the absence of Upa2.

241 Observation of endosomal shuttling of Rrm4-Gfp, Pab1-Gfp, Upa1-Gfp and Rab5a-Gfp
242 revealed that loss of Upa2 caused a slight increase in the velocity and amount of shuttling
243 signals (Figure 6G-I, Supplementary Videos V10-13). There was only one exception: the
244 amount of Pab1-containing endosomes was reduced to about 50%, suggesting that Upa2 is
245 needed for a stable interaction of Pab1-containing mRNAs on endosomes. This is consistent
246 with the reduced shuttling range of *cdc3*^{B16} mRNA as described above and the observation that
247 Cdc3-Gfp protein is no longer present on endosomes in the absence of Upa2 (Zander et al.,
248 2016; see Discussion). Importantly, Upa2 is essential for the correct association of mRNAs,
249 Pab1, as well as Rrm4, on endosomes. Thus, we identified an endosome-specific and
250 functionally important factor that functions as novel core component of endosomal mRNA
251 transport.
252

253 **Discussion**

254 Functional units of mRNA transport are higher-order mRNPs consisting of cargo mRNAs,
255 RNA-binding proteins and additional interacting proteins (Mofatteh & Bullock, 2017). A
256 crucial task is to differentiate between core components that are essential to orchestrate
257 transport, and accessory components. The latter might mediate for example translational
258 regulation of cargo mRNAs. Here, we identified Upa2 as a novel core component of endosomal
259 mRNA transport. This interactor of the poly(A)-binding protein appears to stabilise higher-
260 order endosomal mRNPs during transport suggesting that it functions as a scaffold protein
261 (Figure 7).

262 **A novel multi PAM2 protein for endosomal mRNA transport**

263 Upa2 is a large protein of 232 kDa that contains four functional PAM2 motifs for interaction
264 with the C-terminal MLLE domain of Pab1. It is known from earlier structural studies that the
265 C-terminal MLLE domain of human PABC1 forms a defined peptide pocket to accommodate

266 various PAM2 sequences (Kozlov et al., 2001). Currently, only three MLLE-containing
267 proteins are described: the poly(A)-binding protein, the E3 ubiquitin ligase UBR5 and mRNA
268 transporter Rrm4. UBR5 is a HECT-type (homologous to the E6AP C terminus) ligase that
269 functions in translational regulation and microRNA-mediated gene silencing (Su et al., 2011).
270 The PAM2 motif is present in various PABC1-interaction partners such as eRF3, GW182
271 and PAN3 functioning in various steps of posttranscriptional control such as translation,
272 miRISC assembly and deadenylation, respectively (Xie et al., 2014). The vast majority of
273 proteins harbour a single PAM2 motif, only eRF3 and Tob contain two overlapping PAM2
274 motifs for MLLE interaction (Kozlov & Gehring, 2010, Ezzeddine et al., 2007). Therefore, it
275 is exceptional to find four PAM2 motifs in Upa2 and due to the potential dimerisation via its
276 C-terminal coiled coil region Upa2 offers an extensive interaction platform for Pab1 (Figure 7).
277 Experimental evidence confirmed that the PAM2 motifs of Upa2 interact with Pab1.
278 However, it seems to be an utter paradox that these evolutionarily conserved PAM2 motifs are
279 not important for the function of Upa2 during endosomal mRNA transport. The same holds true
280 for Upa1, where the PAM2 motif is also dispensable for function (Pohlmann et al., 2015). A
281 possible explanation is a high level of redundancy. This is supported by the fact that in
282 endosomal mRNPs there are verified PAM2 motifs in Upa1 and Upa2 as well as additional
283 cryptic versions in Rrm4. It is conceivable that all PAM2 sequences and their variants must be
284 mutated to observe defects in mRNA transport and consequently in hyphal growth. In fact,
285 redundancy was already observed during the study of PAM2-like motifs. Only deletion of both
286 PAM2-like sequences in Upa1 resulted in loss of function (Pohlmann et al., 2015).
287 Alternatively, we might not be able to detect the functional significance of the PAM2 / Pab1
288 interaction under optimal laboratory conditions. The interaction could be of specific importance
289 under certain stress conditions. Comparably, a function of the small Glycine rich protein Grp1
290 was only observed during hyphal growth under cell wall stress conditions (Olgeiser et al. *in*
291 *revision*).

292 Besides PAM2 motifs and a coiled coil region for dimerization, we identified two
293 additional functionally important regions. Firstly, we succeeded in mapping a novel N-terminal
294 effector domain. Interestingly, this domain is embedded in a part of the protein that is predicted
295 to be rich in intrinsically disordered regions (IDRs; Supplementary Figure S5). In the future,
296 we need to carry out an extensive fine mapping to identify clear boundaries of this domain and
297 identify the respective interaction partner. Secondly, we discovered a C-terminal GWW motif
298 that is essential for the endosomal localisation of Upa2. Since the presence of Upa2 depends on
299 the RNA-binding capacity of Rrm4, we assume that the GWW motif does not bind endosomal
300 lipids directly. Most likely, it interacts with a protein component of endosomal mRNPs
301 (Figure 7). This assumption is supported by the fact that an evolutionarily conserved GWW
302 motif at the C-terminus of bacterial endoribonuclease RNase E interacts with a peptide-binding
303 pocket of a PNPase (exoribonuclease polynucleotide phosphorylase; Hardwick et al., 2011,
304 Hardwick et al., 2012). Furthermore, GWW motifs have been implicated in intramolecular
305 interactions of two SH3 domains of the NADPH oxidase component $p47^{phox}$ (Groemping et al.,
306 2003). Related dispersed GW motifs in the posttranslational regulator GW182 mediate
307 recruitment of CCR4-NOT deadenylation components during miRNA-mediated repression
308 (Chekulaeva et al., 2011). In essence, we identified at least four different types of interfaces for
309 protein/protein interactions in Upa2 supporting the hypothesis that it serves as a scaffold
310 protein.

311 **The function of Upa2 during endosomal transport**

312 In order to study the function of Upa2 *in vivo* we combined genetic with cell biological
313 approaches. Loss of Upa2 causes the same aberrant growth phenotype and reduced Cts1
314 secretion as observed in *rrm4*Δ and *upa1*Δ strains (König et al., 2009, Pohlmann et al., 2015),
315 suggesting that these proteins function in the same pathway. This is supported by a phylogenetic
316 analysis showing the co-appearance of all three proteins.

317 The bipolar hyphal growth phenotype can in part be explained by the defects in forming
318 the gradient of septin filaments at the growth pole, since septins are important during the initial
319 phase of unipolar hyphal growth (Baumann et al., 2014, Zander et al., 2016). The formation of
320 the septin gradient depends on the endosomal transport of septin heteromers and in turn
321 heteromer assembly depends on endosomal transport of the septin encoding mRNAs (Baumann
322 et al., 2014, Zander et al., 2016). Thus, the most rational explanation for the observed defects
323 in hyphal growth in *upa2*Δ strains is the reduced transport of septin mRNAs resulting in fewer
324 septin proteins on endosomes. Since the presence of the different septins on transport
325 endosomes are interdependent (Zander et al., 2016), the reduced amount might not be able to
326 support endosomal assembly and localisation of septin proteins causing the observed defects in
327 septin gradients. The hypothesis of local translation on the endosomal surface for septin
328 assembly (Baumann et al., 2014, Zander et al., 2016) has recently been supported by the finding
329 that most heteromeric protein complexes are co-translationally assembled in eukaryotes (Shiber
330 et al., 2018).

331 Loss of Upa2 also causes a slight increase in the amount and velocity of transport
332 endosomes suggesting that the absence of Upa2 and the reduced associated mRNA cargos has
333 an influence on transport endosomes in general. However, the most profound differences were
334 recognized studying the mRNP components Rrm4 and Pab1. We observed an aberrantly strong
335 formation of Rrm4 on microtubules and reduced endosomal localisation of Pab1. Hence, Upa2
336 appears to be crucial for the stable association of mRNPs on the surface of endosomes during
337 transport. This is consistent with important key findings of this study that Upa2, like Rrm4,
338 specifically localises to transport endosomes and that it is present an almost all transport
339 endosomes. In conjunction with the aforementioned scaffolding function, Upa2 fulfils the
340 necessary criteria to function as a novel core component of endosomal mRNP transport.

341 **Conclusions**

342 In recent years the identification of components of the endosomal mRNA transport machinery
343 in *U. maydis* has advanced significantly (Figure 7). Importantly, it is the first system, where a
344 transcriptome-wide binding landscape of the key RBP is available. Comparing bound RNAs of
345 Rrm4 with the accessory component Grp1 revealed that Rrm4 orchestrates a tailored transport
346 strategy for distinct sets of cargo mRNAs (Olgeiser et al., in revision). Here, we add the
347 evolutionarily conserved Upa2 as an important novel piece to our jigsaw puzzle of endosomal
348 mRNA transport.

349 Key concepts appear to be conserved throughout evolution and might also be applicable to
350 higher eukaryotes. In fungi, for example, Rrm4, Upa1 and Upa2 are conserved throughout
351 Basidiomycetes suggesting that endosomal mRNA transport is more wide-spread than currently
352 anticipated (J. Müller, T. Pohlmann and M. Feldbrügge, unpublished). Consistently, in animal
353 systems, endosomal components have been implicated in mRNA transport during axonal
354 growth (Falk et al., 2014, Konopacki et al., 2016) and mRNAs associated with Rab5-positive
355 endosomes were recently discovered in plants (Yang et al., 2018). Finally, discovering the key
356 RNA-binding protein Rrm4 that is linked intensively and intimately with endosomal
357 membranes fits to the new emerging concept that RNA and membrane biology are tightly
358 intertwined. Membrane-associated RBPs (memRBPs) are most likely important at all
359 intracellular membranes to orchestrate spatio-temporal expression (Béthune et al. *in revision*).
360 These findings stress the vital role of *U. maydis* as a model for RNA biology (Haag et al., 2017,
361 Niessing et al., 2018).

362

363 **Materials and methods**

364 **Plasmids, strains and growth conditions**

365 For cloning of plasmids and GST pulldown experiments, *E. coli* Top10 cells (Life
366 Technologies, Carlsbad, CA, USA) and *E. coli* Rosetta2 pLysS (Merck 71403) were used,

367 respectively. Transformation, cultivation and plasmid isolation were conducted using standard
368 techniques. All *U. maydis* strains are derivatives of AB33, in which hyphal growth can be
369 induced (Brachmann et al., 2001). Yeast-like cells were incubated in complete medium (CM)
370 supplemented with 1% glucose, whereas hyphal growth was induced by changing to nitrate
371 minimal medium (NM) supplemented with 1% glucose, both at 28°C (Brachmann et al., 2001).
372 Detailed growth conditions and cloning strategies for *U. maydis* are described elsewhere
373 (Baumann et al., 2012, Brachmann et al., 2004, Terfrüchte et al., 2014). All plasmids were
374 verified by sequencing. Strains were generated by transforming progenitor strains with
375 linearised plasmids. Successful integration of constructs was verified by diagnostic PCR and
376 by Southern blot analysis (Brachmann et al., 2004). For ectopic integration, plasmids were
377 linearised with SspI and targeted to the ip^S locus (Loubradou et al., 2001). Wild-type strain
378 UM521 genomic DNA was used as a template for PCR amplifications of ORFs, unless
379 otherwise stated. Yeast two-hybrid tests were carried out using *S. cerevisiae* strain AH109
380 (Clontech Laboratories Inc., Mountain View, CA, USA). A detailed description of all plasmids
381 and strains is given in Supplementary Tables T1 to T6. Sequences are available upon request.

382 **Microscopy, image processing and image analysis**

383 Laser-based epifluorescence-microscopy was performed on a Zeiss Axio Observer.Z1 equipped
384 with CoolSNAP HQ2 CCD (Photometrics, Tuscon, AZ, USA) and ORCA-Flash4.0 V2+
385 CMOS (Hamamatsu Photonics Deutschland GmbH, Geldern, Germany) cameras. For
386 excitation we used a VS-LMS4 Laser-Merge-System (Visitron Systems, Puchheim, Germany)
387 that combines solid state lasers for excitation of Gfp (488 nm at 50 or 100 mW) and
388 Rfp/mCherry (561 nm at 50 or 150 mW).

389 For the quantification of unipolar hyphal growth, cells were grown in 20 ml cultures to an
390 OD_{600} of 0.5 and hyphal growth was induced. After 6 hours, more than 100 cells per experiment
391 were imaged and analysed for growth behaviour. Cells were scored for unipolar and bipolar

392 growth as well for formation of empty sections. At least three independent experiments were
393 conducted.

394 For analysis of signal number and velocity, we recorded videos with an exposure time of
395 150 ms and 150 frames taken. All videos and images were processed and analysed using
396 Metamorph (Version 7.7.0.0, Molecular Devices, Seattle, IL, USA). Kymographs were
397 generated using a built-in plugin and processively moving particles (covered distance of hypha
398 per 22.5 s < 50 µm) were counted manually. The average velocity was determined by
399 quantifying processive signals (movement > 5 µm). Data points represent means from three
400 independent experiments (n = 3) with mean of means (red line) and s.e.m. For each experiment
401 at least 30 signals per hypha were analysed out of 10 hyphae per strain.

402 For quantification of Cdc3 fluorescence intensity line-scans were conducted in a region of
403 10 µm from hyphal tips. Relative fluorescence intensities of < 28 hyphal tips were averaged.

404 Colocalization studies of dynamic processes were carried out by using a two-channel
405 imaging system (DV2, Photometrics, Tucson, AZ, USA; Baumann et al., 2016, Pohlmann et
406 al., 2015).

407 **RNA live imaging, FM4-64 staining and benomyl treatment**

408 RNA imaging in living cells was conducted by using the improved λN*-based green-RNA
409 method described previously (Pohlmann et al., 2015). For RNA visualization a modified λN
410 (λN*) was fused to three copies of enhanced Gfp as well as to a nuclear localization signal
411 (NLS) and 16 copies of the boxB loop were inserted in the *cdc3* mRNA. Both constructs were
412 under the control of the constitutive active promoter P_{otef}. For each experiment, >18 hyphae
413 were analysed per strain. Statistical tests were performed using Graphpad Prism5 (version 5.00;
414 Graphpad Software, La Jolla, CA, USA). A detailed protocol for subsequent data analysis was
415 described elsewhere (Zander et al., 2016). For staining of cells with FM4-64, a 1 ml sample of
416 hyphal cells was labelled with 0.8 µM FM4-64 (Thermo Fisher, Waltham, MA, USA). After

417 incubation for 1 min at room temperature, the labelled cells were analysed by fluorescence
418 microscopy. For benomyl treatment, a 1 ml sample of hyphal cells was treated with 20 µM
419 benomyl (Sigma-Aldrich, Taufkirchen, Germany). After incubation for 30 min at room
420 temperature with agitation samples were analysed by microscopy.

421 **Fluorimetric measurement of chitinolytic activity**

422 Chitinolytic activity measurements of *U. maydis* cells were carried out as described elsewhere
423 (Koepke et al., 2011, Pohlmann et al., 2015). Briefly, *U. maydis* cell suspensions were grown
424 to an OD_{600} of 0.5. The culture was divided in half, yeast-like growing cells were measured
425 directly while activity of hyphae was measured 6 h after induction of hyphal growth. 30 µl of
426 the culture were mixed with 70 µl 0.25 µM 4-Methylumbelliferyl-
427 β-D-N,N‘,N‘‘-triacetylchitotrioside (MUC, Sigma-Aldrich, Taufkirchen, Germany), a
428 fluorogenic substrate for chitinolytic activity. After incubation for 1 h, the reaction was stopped
429 by addition of 200 µl 1M Na_2CO_3, followed by detection of the fluorescent product with the
430 fluorescence spectrometer Infinite M200 (Tecan Group Ltd., Männedorf, Switzerland) using an
431 excitation and emission wavelength of 360 nm and 450 nm, respectively. Chitinase activity was
432 set and reported in relation to AB33 (wt) activity. Five independent biological experiments were
433 performed with three technical replicates per strain.

434 **Yeast two-hybrid analysis**

435 The yeast two-hybrid analyses were carried out as described elsewhere (Pohlmann et al., 2015).
436 Briefly, using the two-hybrid system Matchmaker 3 from Clontech, strain AH109 was co-
437 transformed with derivates of pGBKT7-DS and pGADT7-Sfi (Supplementary Table T4) and
438 cells were grown on synthetic dropout (SD) plates without leucine and tryptophan at 28° C for
439 4 days. Subsequently, colonies were patched on SD plates without leucine and tryptophan
440 (control) or on SD plates without leucine, tryptophan, histidine and adenine (selection). Plates
441 were incubated at 28°C for 3 days to test for growth under selection condition. For qualitative

442 plate assays cells were cultivated in SD without leucine and tryptophan to OD_{600} of 0.5 and
443 successively diluted with sterile water in four steps at 1:5 each. 4 µl were spotted on control as
444 well as selection plates and incubated at 28° C for 3 days. Colony growth was documented with
445 a LAS 4000 imaging system (GE Healthcare Life Sciences, Little Chalfont, UK).

446 **Protein extracts and Western blot analysis**

447 *U. maydis* hyphae were harvested 6 hours post induction (h.p.i.) by centrifugation (7546 x g,
448 10 minutes) and resuspended in 2 ml l-arginine rich buffer (0.4 M sorbitol; 5 % glycerol; 50
449 mM Tris/HCl pH7.4; 300 mM NaCl; 1 mM EDTA; 0.5% Nonidet P-40; 0.1% SDS; 72.5 mM
450 l-arginine; 1 tablet of complete protease inhibitor per 25 ml, Roche, Mannheim, Germany;
451 1 mM DTT; 0.1 M PMSF; 0.5 M benzamidine). Cells were lysed in a Retsch ball mill (MM400;
452 Retsch, Haan, Germany) while keeping samples constantly frozen using liquid nitrogen. 2 ml
453 cell suspension per grinding jar with two grinding balls (d = 12 mm) were agitated for 2 x 10
454 minutes at 30 Hertz. Protein concentrations were measured by Bradford assay (Bio-Rad,
455 Munich, Germany). For Western Blot analysis, 80 µg of protein were heated to 60°C for 10
456 minutes, resolved by 8% SDS-PAGE and transferred to a nitrocellulose membrane (GE
457 Healthcare, Munich, Germany) by semi-dry blotting. Membranes were probed with α-Gfp
458 (Roche, Freiburg, Germany) and α-actin (MP Biomedicals, Eschwege, Germany) antibodies.
459 As secondary antibody a mouse IgG HRP conjugate was used (Promega, Madison, WI, USA).
460 Detection was carried out by using AceGlow (VWR Peqlab, Erlangen, Germany).

461 **GST pull down experiments**

462 Derivatives of plasmids pGEX and pET15B (Supplementary Table T5) were transformed into
463 *E. coli* Rosetta2 pLysS (Merck 71403). Overnight cultures were diluted 1:50 in a final volume
464 of 50 ml. Protein expression was induced with 1mM IPTG for 4 h at 28°C. Cells were pelleted,
465 resuspended in 10 ml lysis buffer and lysed by sonication. Cell lysate was centrifuged at
466 16,000 g for 15 minutes and the supernatant was transferred to the fresh microcentrifuge tubes.

467 50 µl glutathione beads (GE Healthcare) were transferred to a new 1.5 ml microcentrifuge tube
468 and washed 3 times with 1 ml lysis buffer (20 mM Tris-Cl, pH 7.5; 200 mM NaCl; 1mM EDTA,
469 pH 8.0; 0.5 % Nonidet P-40; 1 tablet complete protease inhibitor per 50ml, Roche, Mannheim,
470 Germany). For each pulldown, 1 ml of supernatant of GST-tagged protein was added to the
471 washed beads, incubated for 1 h at 4° C and subsequently washed 5 times with 1 ml lysis buffer.
472 1 ml supernatant containing His-tagged Upa2 variant was added directly to the washed GST
473 bead and incubated for 1 h at 4° C and subsequently washed 5 times with lysis buffer. The beads
474 were boiled for 6 min at 99° C in 100 µl of 1x Laemmli buffer. 10 µl of each GST-pulldown
475 fraction was analysed by SDS-PAGE and Coomassie blue (CBB R250) staining. 1 ml
476 supernatant containing Upa2 variant was added directly to the washed Ni-NTA (Macherey-
477 Nagel) bead, incubated for 1 h at 4° C and subsequently washed 5 times with 1 ml lysis buffer.
478 20 µl of each Upa2 variants were loaded on control lanes in SDS PAGE as an input. Note, that
479 the input fraction "H" shows Ni-NTA precipitated Upa2, which could not be visualized before
480 enrichment.

481 For Western blotting protein samples were resolved by 10% SDS-PAGE and transferred
482 to a PVDF membrane (GE Healthcare) by semi-dry blotting. Western blot analysis was
483 performed with α-GST (Sigma G7781), α-His (Sigma H1029). α-Rabbit IgG HRP conjugate
484 (Promega W4011), α-mouse IgG HRP conjugate (Promega W4021) were used as secondary
485 antibodies. Activity was detected using the AceGlow blotting detection system (VWR Peqlab,
486 Erlangen, Germany).

487 **Phylogenetic analysis and bioinformatics**

488 Sequence data for *U. maydis* genes was retrieved from the PEDANT database
489 (http://pedant.gsf.de/). Accession numbers of *U. maydis* genes used in this study: *upa2*
490 (UMAG_10350), *rrm4* (UMAG_10836), *pab1* (UMAG_03494), *upa1* (UMAG_12183), *rab5a*
491 (UMAG_10615) and *cdc3* (UMAG_10503). Orthologs were identified using fungiDB

492 (Basenko et al., 2018, Stajich et al., 2012), Ensembl Fungi (Kersey et al., 2018) and NCBI
493 blastp tool (Altschul et al., 1990). Sequences alignments were performed with ClustalX (version
494 2.0.12; Larkin et al., 2007). Domains were predicted using SMART (Letunic & Bork, 2018,
495 Schultz et al., 1998), conserved domain database from the NCBI (CDD; Marchler-Bauer et al.,
496 2017) and active search using ScanProsite (de Castro et al., 2006). The coiled coil dimerisation
497 domain was predicted using the Interpro COILS program (Lupas et al., 1991). The phylogenetic
498 tree is based on the NCBI taxonomy and was created using phyloT online tool
499 (phylot.biobyte.de). The lengths of the lines do not represent evolutionary distance. The
500 accession numbers for the proteins can be found in Supplementary Table T7).

501 Intrinsically disordered regions were predicted using the PONDR VL3-BA algorithm
502 (www.pondr.com, Molecular Kinetics, Inc., IN, USA). VL3-BA is a feedforward neural
503 network predictor generating outputs between 0 and 1 which are smoothed over a sliding
504 window of 9 amino acids. Regions with values of 0.5 or above are considered disordered and
505 are marked in red, while peptide regions with values lower than 0.5 are considered ordered and
506 are marked in blue.

507

508 **Acknowledgements**

509 We acknowledge Drs. A. Brachmann, J. Béthune, K. Zarnack and lab members for discussion
510 and reading of the manuscript. We are grateful to U. Gengenbacher for excellent technical
511 assistance. The work was funded by grants from the Deutsche Forschungsgemeinschaft to MF
512 (FE448/5-2 DFG-FOR1334; FE448/10-1 DFG-FOR2333; DFG-CRC1208 and CEPLAS
513 EXC1028).

514

515 **Conflict of interest**

516 The authors declare that they have no conflict of interest.

517

518 **References**

519 Altschul SF, Gish W, Miller W, Myers EW, Lipman DJ (1990) Basic local alignment search
520 tool. J Mol Biol 215: 403-410
521 Basenko EY, Pulman JA, Shanmugasundram A, Harb OS, Crouch K, Starns D, Warrenfeltz S,
522 Aurrecoechea C, Stoeckert CJ, Jr., Kissinger JC, Roos DS, Hertz-Fowler C (2018)
523 FungiDB: An Integrated Bioinformatic Resource for Fungi and Oomycetes. J Fungi 4: e39
524 Baumann S, König J, Koepke J, Feldbrügge M (2014) Endosomal transport of septin mRNA
525 and protein indicates local translation on endosomes and is required for correct septin
526 filamentation. EMBO Rep 15: 94-102
527 Baumann S, Pohlmann T, Jungbluth M, Brachmann A, Feldbrügge M (2012) Kinesin-3 and
528 dynein mediate microtubule-dependent co-transport of mRNPs and endosomes. J Cell Sci
529 125: 2740-2752
530 Baumann S, Takeshita N, Grün N, Fischer R, Feldbrügge M (2015) Live cell imaging of
531 endosomal trafficking in fungi. In Methods in Mol Biol: Membrane trafficking, Tang BL
532 (ed) pp 347-363. New York: Springer
533 Baumann S, Zander S, Weidtkamp-Peters S, Feldbrügge M (2016) Live cell imaging of septin
534 dynamics in *Ustilago maydis*. In Septins, Gladfelter AS (ed) pp 143-149. Elsevier Inc.
535 Becht P, König J, Feldbrügge M (2006) The RNA-binding protein Rrm4 is essential for polarity
536 in *Ustilago maydis* and shuttles along microtubules. J Cell Sci 119: 4964-4973
537 Brachmann A, König J, Julius C, Feldbrügge M (2004) A reverse genetic approach for
538 generating gene replacement mutants in *Ustilago maydis*. Mol Gen Genom 272: 216-226
539 Brachmann A, Weinzierl G, Kämper J, Kahmann R (2001) Identification of genes in the bW/bE
540 regulatory cascade in *Ustilago maydis*. Mol Microbiol 42: 1047-1063
541 Chekulaeva M, Mathys H, Zipprich JT, Attig J, Colic M, Parker R, Filipowicz W (2011)
542 miRNA repression involves GW182-mediated recruitment of CCR4-NOT through
543 conserved W-containing motifs. Nat Struct Mol Biol 18: 1218-1226

544 de Castro E, Sigrist CJ, Gattiker A, Bulliard V, Langendijk-Genevaux PS, Gasteiger E, Bairoch
545 A, Hulo N (2006) ScanProsite: detection of PROSITE signature matches and ProRule-
546 associated functional and structural residues in proteins. Nucleic Acids Res 34: W362-5
547 Edelmann FT, Schlundt A, Heym RG, Jenner A, Niedner-Boblenz A, Syed MI, Paillart JC,
548 Stehle R, Janowski R, Sattler M, Jansen RP, Niessing D (2017) Molecular architecture and
549 dynamics of *ASH1* mRNA recognition by its mRNA-transport complex. Nat Struct Mol
550 Biol 24: 152-161
551 Eliscovich C, Singer RH (2017) RNP transport in cell biology: the long and winding road.
552 Current opinion in cell biology 45: 38-46
553 Ezzeddine N, Chang TC, Zhu W, Yamashita A, Chen CY, Zhong Z, Yamashita Y, Zheng D,
554 Shyu AB (2007) Human TOB, an antiproliferative transcription factor, is a poly(A)-
555 binding protein-dependent positive regulator of cytoplasmic mRNA deadenylation.
556 Molecular and cellular biology 27: 7791-7801
557 Falk J, Konopacki FA, Zivraj KH, Holt CE (2014) Rab5 and Rab4 regulate axon elongation in
558 the Xenopus visual system. J Neurosci 34: 373-391
559 Groemping Y, Lapouge K, Smerdon SJ, Rittinger K (2003) Molecular basis of phosphorylation-
560 induced activation of the NADPH oxidase. Cell 113: 343-355
561 Haag C, Pohlmann T, Feldbrugge M (2017) The ESCRT regulator Did2 maintains the balance
562 between long-distance endosomal transport and endocytic trafficking. PLoS Genet 13:
563 e1006734
564 Haag C, Steuten B, Feldbrügge M (2015) Membrane-coupled mRNA trafficking in fungi. Annu
565 Rev Microbiol 69: 265-281
566 Hardwick SW, Chan VS, Broadhurst RW, Luisi BF (2011) An RNA degradosome assembly in
567 *Caulobacter crescentus*. Nucleic Acids Res 39: 1449-1459

568 Hardwick SW, Gubbey T, Hug I, Jenal U, Luisi BF (2012) Crystal structure of *Caulobacter*
569 *crescentus* polynucleotide phosphorylase reveals a mechanism of RNA substrate
570 channelling and RNA degradosome assembly. Open biology 2: 120028
571 Higuchi Y, Ashwin P, Roger Y, Steinberg G (2014) Early endosome motility spatially
572 organizes polysome distribution. J Cell Biol 204: 343-357
573 Kersey PJ, Allen JE, Allot A, Barba M, Boddu S, Bolt BJ, Carvalho-Silva D, Christensen M,
574 Davis P, Grabmueller C, Kumar N, Liu Z, Maurel T, Moore B, McDowall MD, Maheswari
575 U, Naamati G, Newman V, Ong CK, Paulini M et al. (2018) Ensembl Genomes 2018: an
576 integrated omics infrastructure for non-vertebrate species. Nucleic Acids Res 46: D802-
577 D808
578 Koepke J, Kaffarnik F, Haag C, Zarnack K, Luscombe NM, König J, Ule J, Kellner R, Begerow
579 D, Feldbrügge M (2011) The RNA-binding protein Rrm4 is essential for efficient secretion
580 of endochitinase Cts1. Mol Cell Proteom 10: M111.011213 1-15
581 König J, Baumann S, Koepke J, Pohlmann T, Zarnack K, Feldbrügge M (2009) The fungal
582 RNA-binding protein Rrm4 mediates long-distance transport of *ubi1* and *rho3* mRNAs.
583 EMBO J 28: 1855-1866
584 Konopacki FA, Wong HH, Dwivedy A, Bellon A, Blower MD, Holt CE (2016) ESCRT-II
585 controls retinal axon growth by regulating DCC receptor levels and local protein synthesis.
586 Open biology 6: 150218
587 Kozlov G, Gehring K (2010) Molecular basis of eRF3 recognition by the MLLE domain of
588 poly(A)-binding protein. PLoS One 5: e10169
589 Kozlov G, Trempe JF, Khaleghpour K, Kahvejian A, Ekiel I, Gehring K (2001) Structure and
590 function of the C-terminal PABC domain of human poly(A)-binding protein. Proc Natl
591 Acad Sci U S A 98: 4409-4413

592 Larkin MA, Blackshields G, Brown NP, Chenna R, McGettigan PA, McWilliam H, Valentin
593 F, Wallace IM, Wilm A, Lopez R, Thompson JD, Gibson TJ, Higgins DG (2007) Clustal
594 W and Clustal X version 2.0. Bioinformatics 23: 2947-2948
595 Letunic I, Bork P (2018) 20 years of the SMART protein domain annotation resource. Nucleic
596 Acids Res 46: D493-D496
597 Loubradou G, Brachmann A, Feldbrügge M, Kahmann R (2001) A homologue of the
598 transcriptional repressor Ssn6p antagonizes cAMP signalling in *Ustilago maydis.* Mol
599 Microbiol 40: 719-730
600 Lupas A, Van Dyke M, Stock J (1991) Predicting coiled coils from protein sequences. Science
601 252: 1162-1164
602 Marchler-Bauer A, Bo Y, Han L, He J, Lanczycki CJ, Lu S, Chitsaz F, Derbyshire MK, Geer
603 RC, Gonzales NR, Gwadz M, Hurwitz DI, Lu F, Marchler GH, Song JS, Thanki N, Wang
604 Z, Yamashita RA, Zhang D, Zheng C et al. (2017) CDD/SPARCLE: functional
605 classification of proteins via subfamily domain architectures. Nucleic Acids Res 45: D200-
606 D203
607 Martin KC, Ephrussi A (2009) mRNA localization: gene expression in the spatial dimension.
608 Cell 136: 719-730
609 Mofatteh M, Bullock SL (2017) SnapShot: Subcellular mRNA localization. Cell 169: 178.e1
610 Niessing D, Jansen RP, Pohlmann T, Feldbrügge M (2018) mRNA transport in fungal top
611 models. Wiley interdisciplinary reviews RNA 9: e1453
612 Pohlmann T, Baumann S, Haag C, Albrecht M, Feldbrügge M (2015) A FYVE zinc finger
613 domain protein specifically links mRNA transport to endosome trafficking. eLife 4:
614 e06041
615 Schultz J, Milpetz F, Bork P, Ponting CP (1998) SMART, a simple modular architecture
616 research tool: identification of signaling domains. Proc Natl Acad Sci U S A 95: 5857-
617 5864

618 Schuster M, Kilaru S, Fink G, Collemare J, Roger Y, Steinberg G (2011) Kinesin-3 and dynein
619 cooperate in long-range retrograde endosome motility along a non-uniform microtubule
620 array. Mol Biol Cell 22: 3645-3657
621 Shiber A, Doring K, Friedrich U, Klann K, Merker D, Zedan M, Tippmann F, Kramer G, Bukau
622 B (2018) Cotranslational assembly of protein complexes in eukaryotes revealed by
623 ribosome profiling. Nature 561: 268-272
624 Stajich JE, Harris T, Brunk BP, Brestelli J, Fischer S, Harb OS, Kissinger JC, Li W, Nayak V,
625 Pinney DF, Stoeckert CJ, Jr., Roos DS (2012) FungiDB: an integrated functional genomics
626 database for fungi. Nucleic Acids Res 40: D675-681
627 Steinberg G, Fuchs U (2004) The role of microtubules in cellular organization and endocytosis
628 in the plant pathogen *Ustilago maydis*. J Microsc 214: 114-123
629 Su H, Meng S, Lu Y, Trombly MI, Chen J, Lin C, Turk A, Wang X (2011) Mammalian
630 hyperplastic discs homolog EDD regulates miRNA-mediated gene silencing. Mol Cell 43:
631 97-109
632 Terfrüchte M, Joehnk B, Fajardo-Somera R, Braus G, Riquelme M, Schipper K, Feldbrügge M
633 (2014) Establishing a versatile Golden Gate cloning system for genetic engineering in
634 fungi. Fungal Genet Biol 62: 1-10
635 Vollmeister E, Schipper K, Baumann S, Haag C, Pohlmann T, Stock J, Feldbrügge M (2012)
636 Fungal development of the plant pathogen *Ustilago maydis*. FEMS Microbiol Rev 36: 59-
637 77
638 Xie J, Kozlov G, Gehring K (2014) The "tale" of poly(A) binding protein: the MLLE domain
639 and PAM2-containing proteins. Biochim Biophys Acta 1839: 1062-1068
640 Yang Y, Chou HL, Crofts AJ, Zhang L, Tian L, Washida H, Fukuda M, Kumamaru T, Oviedo
641 OJ, Starkenburg S, Okita TW (2018) Selective sets of mRNAs localize to extracellular
642 paramural bodies in the rice glup6 mutant line. J Exp Bot 69: 5045-5058

643 Zander S, Baumann S, Weidtkamp-Peters S, Feldbrügge M (2016) Endosomal assembly and
644 transport of heteromeric septin complexes promote septin cytoskeleton formation. J Cell
645 Sci 129: 2778-2792

646

647

648 **Figures 1-7 and Figure legends**

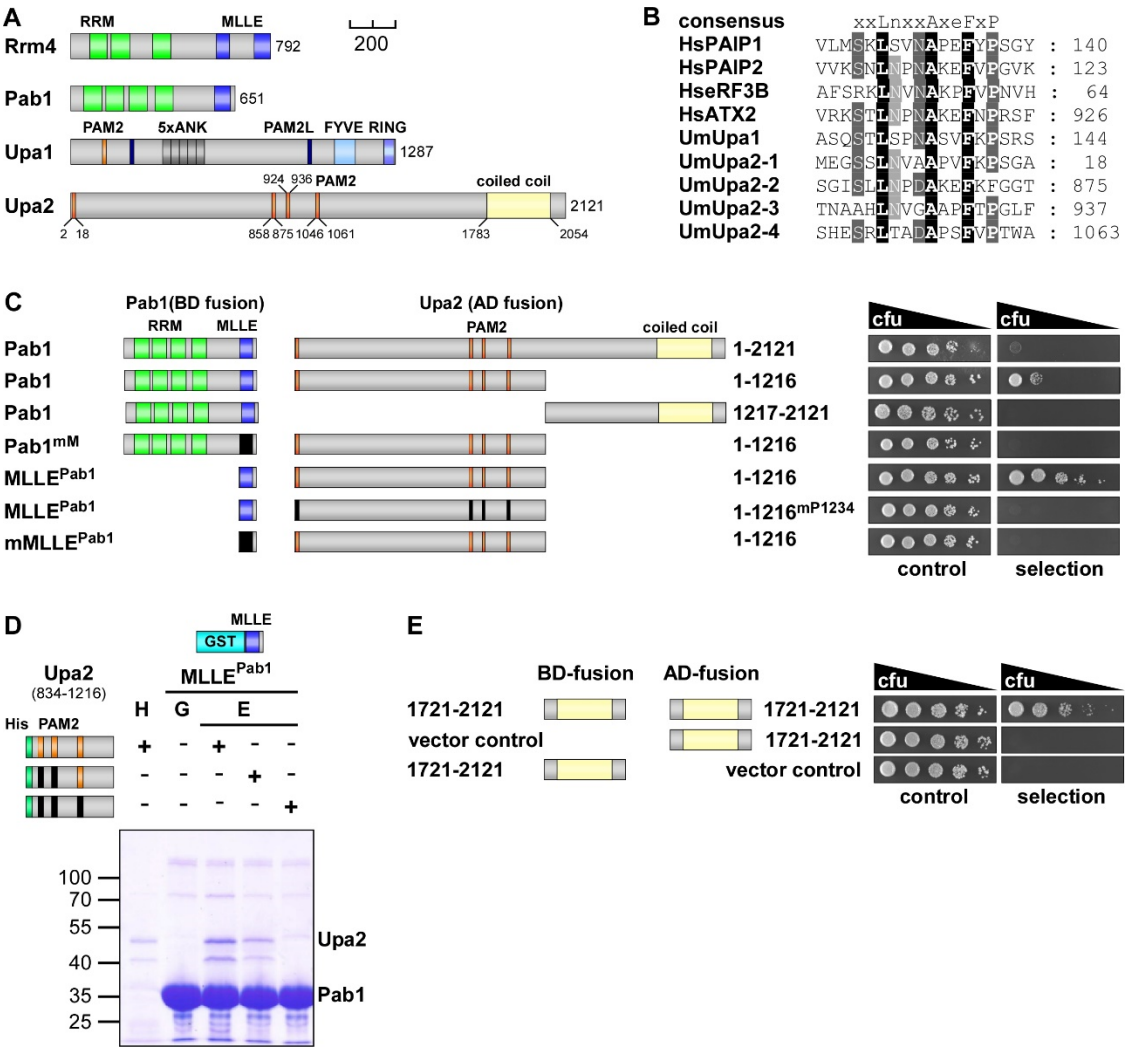

649

650 **Figure 1. Upa2 contains multiple PAM2 motifs for interaction with Pab1.**

651 (**A**) Schematic representation of the MLLE domain-containing proteins Rrm4 and Pab1 as well as the PAM2 motif-
652 containing proteins Upa1 and Upa2 drawn to scale (bar, 200 amino acids; green, RRM domain; blue, MLLE
653 domain; orange, PAM2 motif; dark blue, PAM2-like motif; dark grey, Ankyrin repeats; light blue, FYVE domain;
654 lilac, RING domain; yellow, coiled coil region) (**B**) Comparison of PAM2 sequences found in Upa2 (accession
655 number UMAG_10350) with those of human proteins such as PAIP1 (accession number NP_006442.2), PAIP2
656 (accession number CAG38520.1), eRF3B (accession number CAB91089.1) and ATX2 (accession number
657 NP_002964.3). (**C**) Two-hybrid analysis with schematic representation of protein variants tested on the left. Yeast
658 cultures were serially diluted 1:5 (decreasing colony forming units, cfu) and spotted on respective growth plates
659 controlling transformation and assaying reporter gene expression (see Materials and methods). (**D**) GST co-
660 purification experiments with components expressed in *E. coli*: N-terminal His_6-tagged versions of $Upa2^{834\text{-}1216}$,
661 $Upa2^{834\text{-}1216_mP23}$, and $Upa2^{834\text{-}1216_mP234}$ (amino acids 834–1216; mutation in the PAM2 motifs 2 and 3 as well as
662 2, 3 and 4, respectively; 43 kDa) were tested for binding to the MLLE domain of Pab1 (GST fusion to $MLLE^{Pab1}$;
663 G, input of GST-$MLLE^{Pab1}$). Lane "H" shows Ni-NTA precipitated His_6-Upa2, Lane "G" shows input of
664 $MLLE^{Pab1}$. After GST affinity chromatography proteins were eluted (lanes marked with "E"). Interaction studies
665 were performed with the soluble fraction of protein extracts from *E. coli* to demonstrate specific binding. Note
666 that the Upa2 variants were enriched in the eluate due to the pull down by $MLLE^{Pab1}$. (**E**) Two-hybrid analysis of
667 the coiled coil region of Upa2 (amino acids 1712-2121) fused to binding domain (BD) and activation domain (AD)
668 of the Gal4 transcription factor (design as in C).

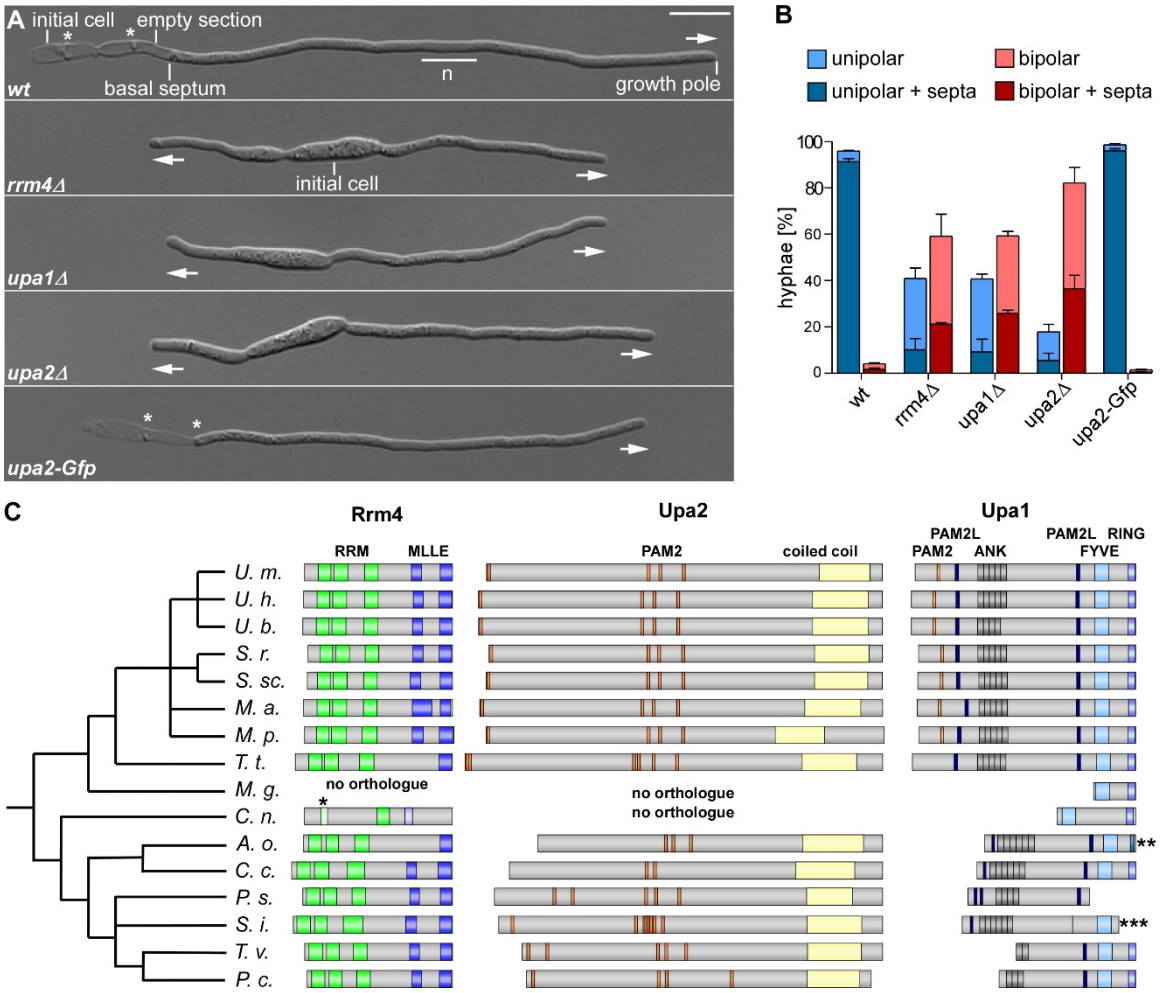

Figure 2. Loss of Upa2 causes defects in hyphal growth.

(**A**) Growth of AB33 derivatives in the hyphal form (6 h.p.i.; growth direction is marked by arrows; n, nucleus; asterisks, basal septa). (**B**) Quantification of hyphal growth (6 h.p.i): unipolarity, bipolarity and septum formation were quantified (error bars, s.e.m.; n = 3 independent experiments, for each experiment >100 hyphae were counted per strain; note that septum formation is given relative to the values of unipolar or bipolar hyphae set to 100%). (**C**) Schematic representation of orthologues of Rrm4, Upa2 and Upa1 in different basidiomycetes. The phylogenetic tree was generated using the phyloT tool using the NCBI taxonomy (no evolutionary distances): U.m.: *Ustilago maydis*, U.h.: *Ustilago hordei*; U.b.: *Ustilago bromivora*; S.r.: *Sporisorium reilianum*; S.sc.: *Sporisorium scitamineum*, M.a.: *Moesziomyces antarcticus*, M.p.: *Melanopsichium pennsylvanicum*, T.t.: *Thecaphora thlaspeos*; M.g.: *Malassezia globosa*; C.n.: *Cryptococcus neoforman var neoformanss*; A.o.: *Armillaria ostoyae*; C.c.: *Coprinopsis cinerea*; P.s.: *Punctularia strigosozonata*; S.i.: *Serendipita indica*; T.v.: *Trametes versicolor*; P.c.: *Phanerochaete carnosa*. * Bioinformatic tools predict weak RRM domains and a non-functional MLLE domain in C.n. Rrm4. ** A.o. Upa1 contains a predicted transmembrane domain instead of a RING domain; *** S.i. Upa1 was manually assembled from two consecutive ORFs. Accession numbers are listed in Supplementary Table T7.

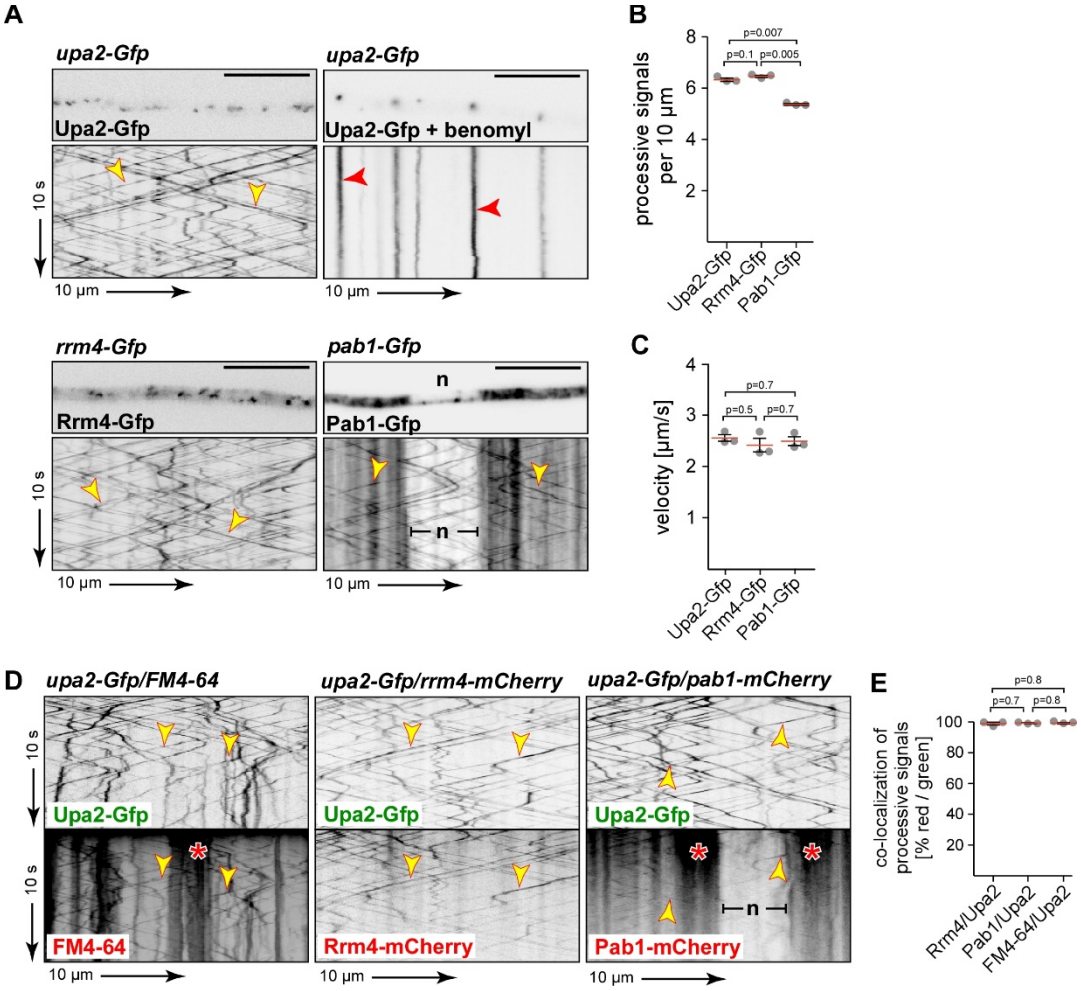

Figure 3. Bidirectional movement of Upa2 on Rrm4-positive endosomes.

(**A**) Micrographs (inverted fluorescence image; size bar, 10 µm) and corresponding kymographs of AB33 hyphae (6 h.p.i.) expressing Upa2-Gfp, Rrm4-Gfp or Pab1-Gfp (arrow length on the left and bottom indicate time and distance, respectively). Bidirectional movement is visible as diagonal lines (yellow arrowheads; n, nucleus; Supplementary Video V1). After addition of the microtubule inhibitor benomyl static signals are seen as vertical lines (red arrowheads; Supplementary Video V1). (**B**) Processive signals per 10 µm of hyphal length (data points representing mean from n = 3 independent experiments, with mean of means, red line, and s.e.m.; paired two-tailed Student´s t-test, for each experiment at least 10 hyphae were analysed per strain). (**C**) Velocity of fluorescent signals (velocity of tracks with > 5 µm processive movement; data points representing means from n = 3 independent experiments, with mean of means, red line, and s.e.m.; paired two-tailed Student´s t-test; for each experiment at least 30 signals per hypha were analysed out of 10 hyphae per strain). (**D**) Kymographs of AB33 hyphae (6 h.p.i.) expressing pairs of red and green fluorescent proteins as indicated. Fluorescence signals were detected simultaneously using dual-view technology (arrow length as in A). Processive co-localising signals are marked by yellow arrowheads. Areas of static signals are indicated by red asterisks (Supplementary Video V2). (**E**) Percentage of processive red fluorescent signals exhibiting co-localisation with the processive green fluorescent signal for strains shown in D (data points represent means set to 100% from n = 3 independent experiments, with mean of means, red line, and s.e.m.; paired two-tailed Student´s t-test; for each experiment 6 hyphae were analysed per strain).

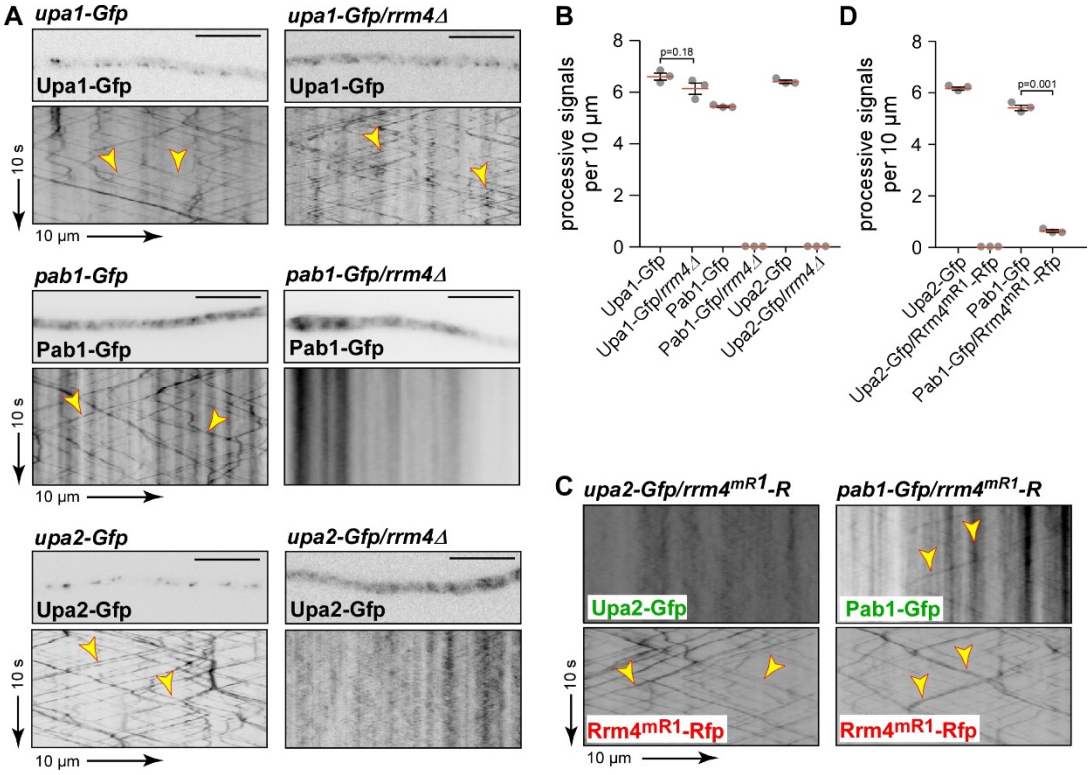

704

705 **Figure 4. Endosomal localisation of Upa2 is mRNA-dependent.**

706 (**A**) Micrographs (inverted fluorescence image; size bar, 10 µm) and corresponding kymographs of AB33 hyphae
707 (6 h.p.i.). Genetic background as indicated above (arrow length on the left and bottom indicate time and distance,
708 respectively). Bidirectional movement is visible as diagonal lines (yellow arrowheads; Supplementary Videos V3-
709 V5). **(B)** Processive signals per 10 µm of hyphal length (data points representing means from n = 3 independent
710 experiments, with mean of means, red line, and s.e.m.; paired two-tailed Student´s t-test, for each experiment at
711 least 10 hyphae were analysed per strain). (**C**) Kymographs of AB33 hyphae (6 h.p.i.) expressing pairs of red and
712 green fluorescent proteins as indicated. Fluorescence signals were detected simultaneously using dual-view
713 technology (arrow length as in A). Processive co-localising signals are marked by yellow arrowheads
714 (Supplementary Videos V6-V7). (**D**) Processive signals per 10 µm of hyphal length (data points representing
715 means from n = 3 independent experiments; with mean of means, red line, and s.e.m.; p value > 0.05; paired two-
716 tailed Student´s t-test, for each experiment at least 10 hyphae were analysed per strain).

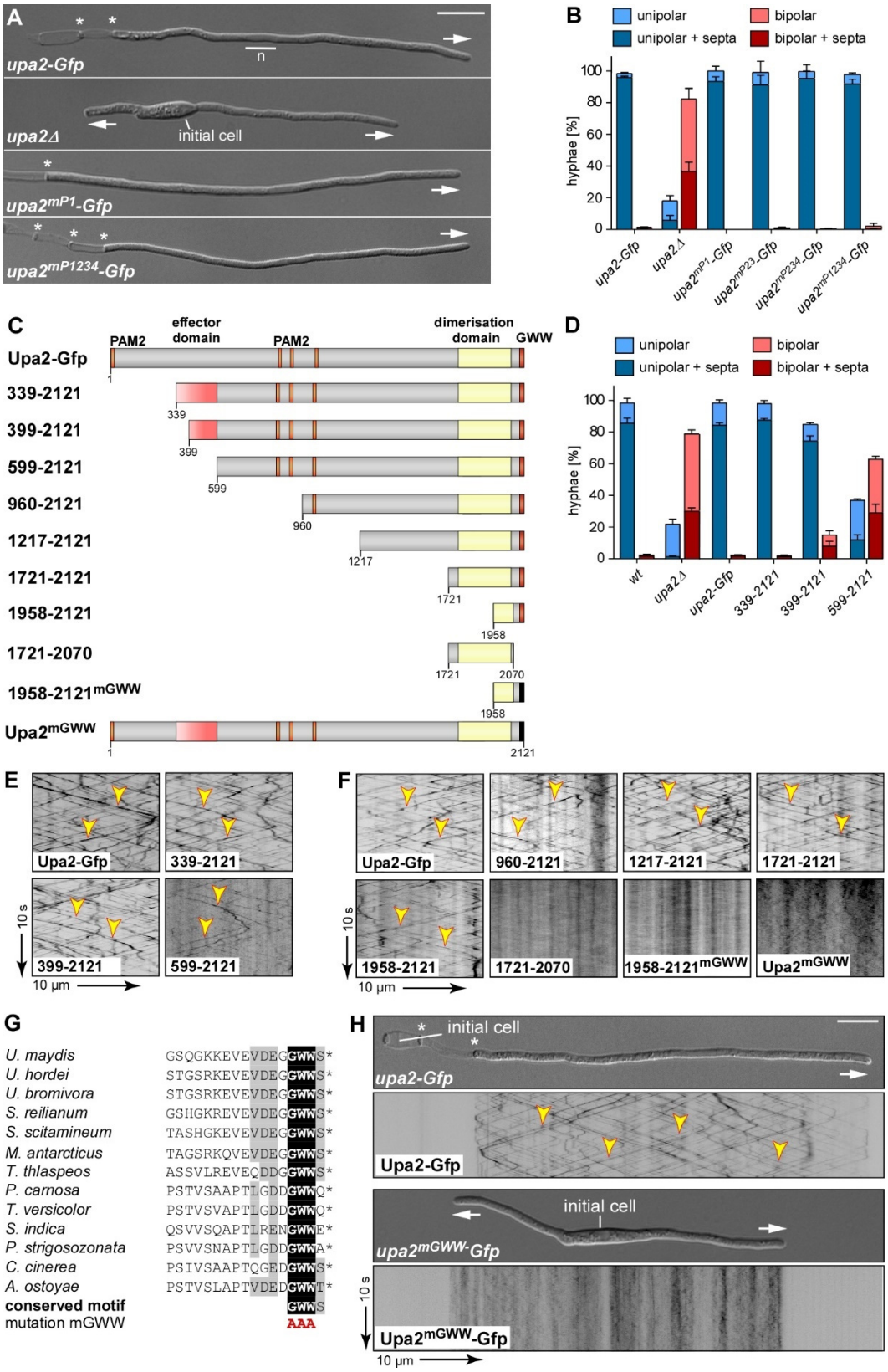

Figure 5. Upa2 carries a functional important effector domain at the N-terminus and a C-terminal GWW motif for endosomal localisation.

(**A**) Growth of AB33 derivatives in the hyphal form (6 h.p.i.; growth direction is marked by arrows; asterisks, basal septa; n, nucleus; size bar 10 µm). (**B**) Quantification of hyphal growth (6 h.p.i): unipolarity, bipolarity and

722 septum formation were quantified (error bars, s.e.m.; n = 3 independent experiments, for each experiment >100
723 hyphae were counted per strain; note that septum formation is given relative to the values of unipolar or bipolar
724 hyphae set to 100%). **(C)** Schematic representation of N-terminal truncations of Upa2 (orange, PAM2 motif; light
725 flow red, effector domain; yellow, dimerization domain; red, GWW; black, mutation in GWW). (**D**) Quantification
726 of hyphal growth of N-terminally truncated Upa2 mutants (6 h.p.i): unipolarity, bipolarity and septum formation
727 were quantified (error bars, s.e.m.; n = 3 independent experiments, for each experiment >100 hyphae were counted
728 per strain; note that septum formation is given relative to the values of unipolar or bipolar hyphae set to 100%).
729 **(E) (F)** Kymographs of AB33 hyphae (6 h.p.i.); genetic background as indicated (arrow length on the left and
730 bottom indicate time and distance, respectively). Bidirectional movement is visible as diagonal lines (yellow
731 arrowheads). **(G)** Comparison of the C-terminal amino acid sequence of Upa2 in *U. maydis* and related fungal
732 species. Accession numbers can be found in Supplementary Table S7. **(H)** Growth of AB33 derivatives in the
733 hyphal form (6 h.p.i.; growth direction is marked by arrows; asterisks, basal septa; size bar, 10 µm) and
734 corresponding kymographs of AB33 hyphae (6 h.p.i.). Genetic background as indicated in left bottom panel (arrow
735 length on the left and bottom indicate time and distance, respectively). Bidirectional movement is visible as
736 diagonal lines (yellow arrowheads; Supplementary Video V8).

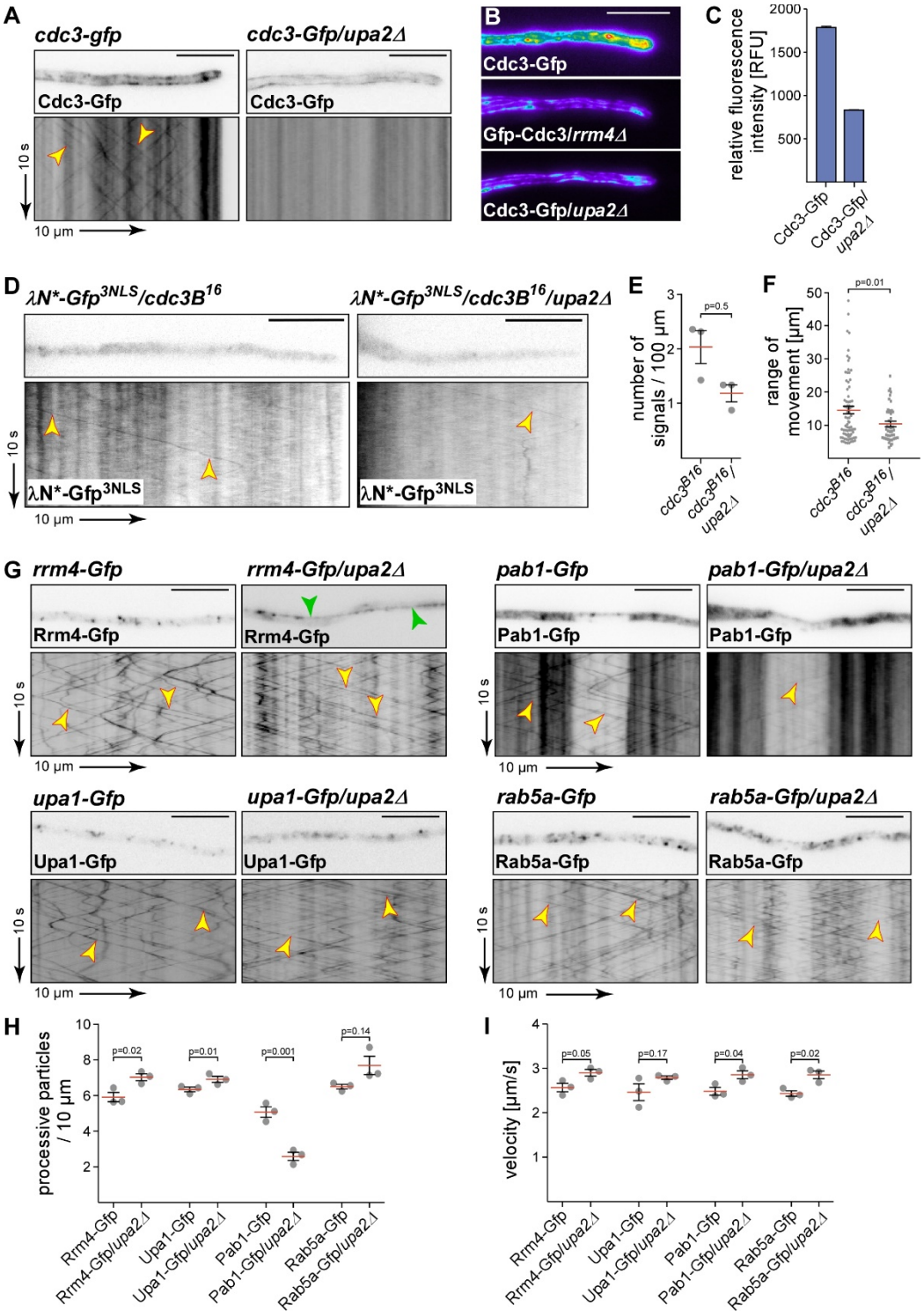

Figure 6. Loss of Upa2 causes defects in the formation of endosomal mRNPs.

(**A**) Micrographs of hyphal tips (inverted fluorescence image; size bar, 10 µm) and corresponding kymographs of AB33 hyphae (6 h.p.i.). Genetic background as indicated above (arrow length on the left and bottom indicate time and distance, respectively). Bidirectional movement is visible as diagonal lines (yellow arrowheads; size bar, 10µm; Supplementary Video V9). (**B**) Heat maps of hyphal tips (6 h.p.i.) of AB33 derivatives expressing Cdc3-Gfp comparing wild type (top panel) with *rrm4Δ* and *upa2Δ* strains (middle, bottom panel), indicating relative fluorescence intensity differences (maximum projection of z-stacks; size bar, 10 µm; red/yellow to green/blue, high to low intensities). (**C**) Relative fluorescence intensity (RFU) (first 10 µm from hyphal tip; mean and error

bars, s.e.m.; n = 3 independent experiments, merged datasets of all values are shown). (**D**) Micrographs of hyphae and corresponding kymographs of AB33 derivatives (8 h.p.i.). Genetic background as indicated above (arrow length on the left and bottom indicate time and distance, respectively). Bidirectional movement of mRNA is visible as diagonal lines (yellow arrowheads; size bar, 10 µm). (**E**) Number of particles per 100 µm hypha (data points representing means from n = 3 independent experiments, with mean of means, red line, and s.e.m.; paired two-tailed Student´s t-test, for each experiment at least 10 hyphae were analysed per strain). (**F**) Scatter plot depicting the range of movement of motile mRNAs (red line, median; n = 3 independent experiments; p value > 0.05; paired Student´s t-test). (**G**) Micrographs of hyphal tips (inverted fluorescence image; size bar, 10 µm) and corresponding kymographs of AB33 hyphae (6 h.p.i.). Genetic background as indicated above (arrow length on the left and bottom indicate time and distance, respectively). Bidirectional movement is visible as diagonal lines (yellow arrowheads; size bar, 10 µm; Supplementary Videos V10-V13). (**H**) Processive signals per 10 µm of hyphal length (data points representing means from n = 3 independent experiments, with mean of means, red line, and s.e.m.; p value > 0.05; unpaired two-tailed Student´s t-test. for each experiment at least 10 hyphae were analysed per strain). (**I**) Velocity of fluorescent signals (velocity of tracks with > 5 µm processive movement; data points representing means from n = 3 independent experiments; with mean of means, red line, and s.e.m.; paired two-tailed Student´s t-test, for each experiment at least 30 signals per hypha were analysed out of 10 hyphae per strain).

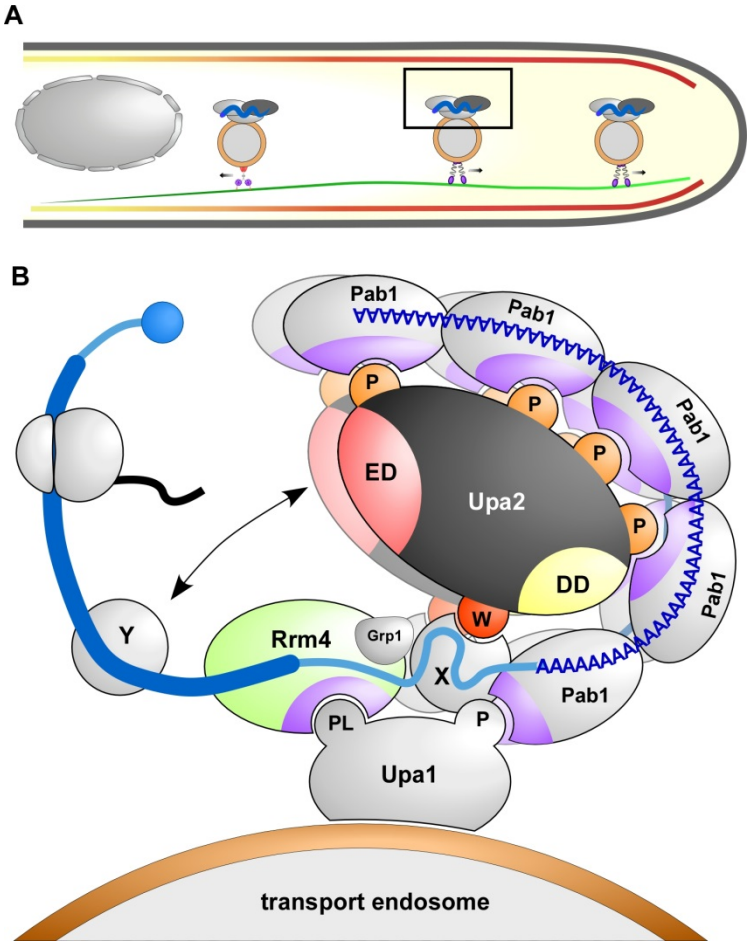

762

763 **Figure 7. Model depicting Upa2 as novel core component of endosomal mRNP transport.**

764 (**A**) Schematic drawing of infectious hypha (red, septin filaments with gradient; green, microtubules; grey circles
765 with golden edge, transport endosomes with mRNPs and molecular motors attached; boxed region is enlarged in
766 B). (**B**) Simplified view of known mRNP components at the cytoplasmic surface of transport endosome and a
767 proposed interplay. Upa2 harbours at least four different protein/protein interfaces: PAM2 motifs (orange), effector
768 domain (light red), dimerisation domain (yellow), GWW motif (dark red). MLLE domains of Pab1 and Rrm4 are
769 given in purple. Additional symbols: 5´ cap, blue circle; mRNA as blue line with ORF (thick line); translating
770 ribosome (grey) with nascent chain (black). Additional mRNP components that are predicted to interact with Upa2
771 are given as grey circles labelled X and Y (for further details, see text).

Supplementary Figures S1-S5

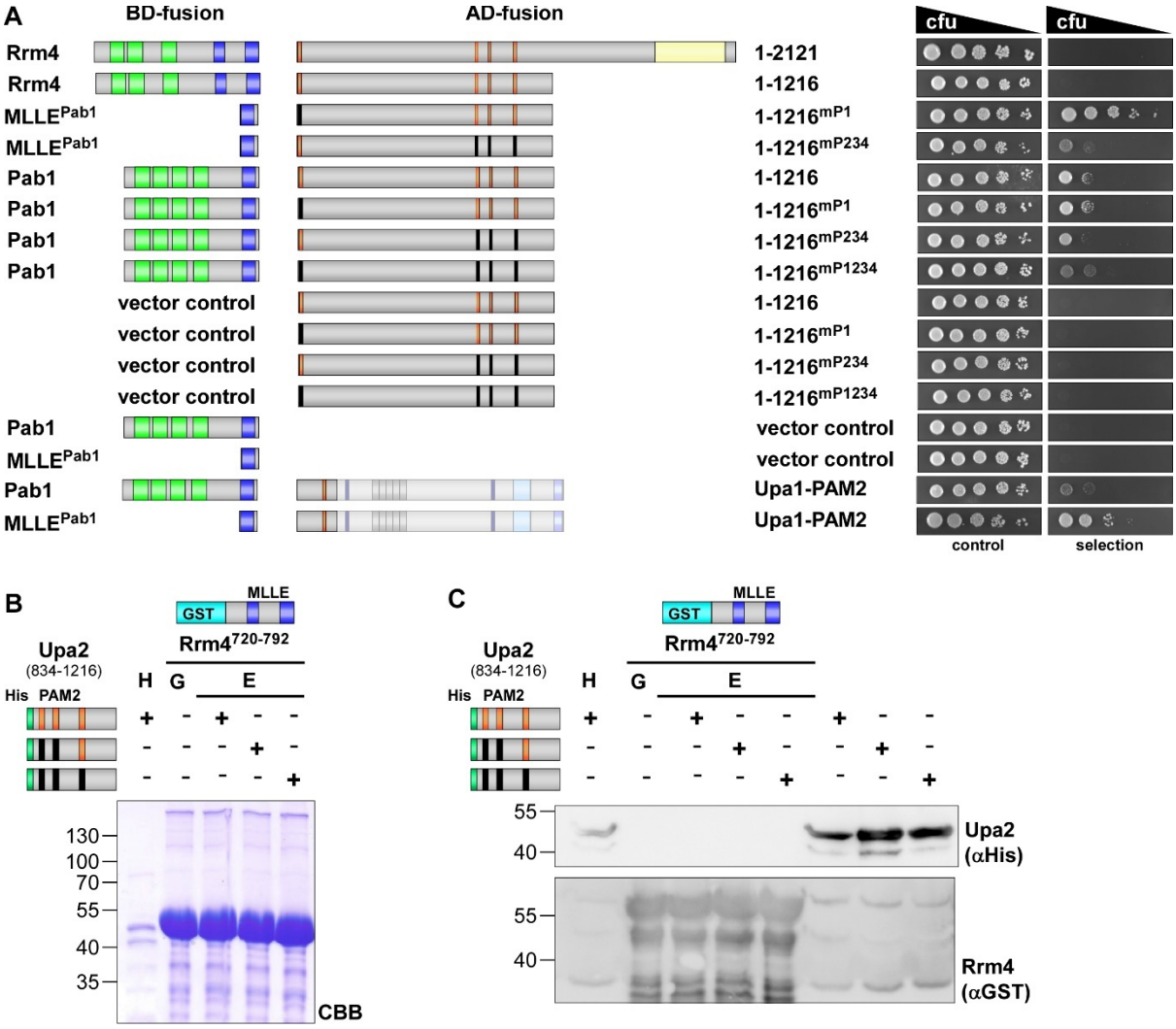

Supplementary Figure S1. PAM2 motifs of Upa2 do not interact with MLLE domains of Rrm4.

(**A**) Two-hybrid analysis with schematic representation of protein variants tested on the left (Colour scheme as in Figure 1A, C). Yeast cultures were serially diluted 1:5 (decreasing colony forming units, cfu) and spotted on respective growth plates controlling transformation and assaying reporter gene expression (see Materials and methods). (**B**) GST co-purification experiments with components expressed in *E. coli*: N-terminal His_6-tagged versions of $Upa2^{834\text{-}1216}$, $Upa2^{834\text{-}1216_mP23}$, and $Upa2^{834\text{-}1216_mP234}$ (amino acids 834–1216; mutation in the PAM2 motifs number 2 and 3 as well as 2, 3 and 4, respectively) were tested for binding to the MLLE domain of Rrm4 (GST fusion to $Rrm4^{720\text{-}792}$ containing two MLLE domains). Lane "H" shows Ni-NTA precipitated His_6-Upa2, lane "G" shows input of GST- $Rrm4^{720\text{-}792}$). After GST affinity chromatography proteins were eluted (lanes marked with "E"). Interaction studies were performed with the soluble fraction of protein extracts from *E. coli* to demonstrate specific binding. (**C**) GST co-purification experiments as shown in B. The absence of $Upa2^{834\text{-}1216}$ interaction with the MLLE domains of Rrm4 was demonstrated in more sensitive Western blot experiments (used antibodies are given on the right). The three lanes on the right show all Upa2 versions after Ni-NTA precipitation.

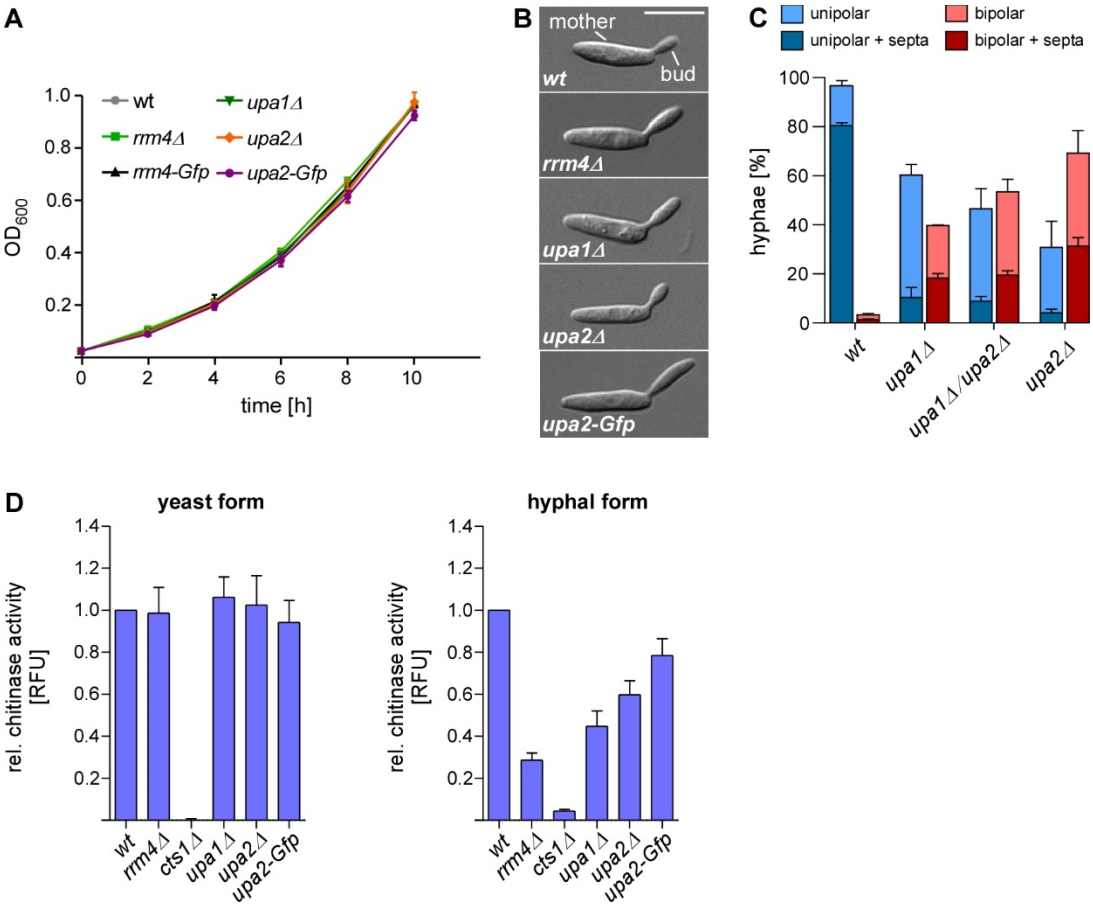

Supplementary Figure S2. Loss of Upa2 causes defects in secretion of chitinase Cts1.

(**A**) Growth of yeast cells of indicated strains in liquid culture. (**B**) DIC images of yeast cells (size bar, 10 µm). (**C**) Quantification of hyphal growth (6 h.p.i): unipolarity, bipolarity and septum formation were quantified (error bars, s.e.m.; n = 3 independent experiments, for each experiment >100 hyphae were counted per strain; note that septum formation is given relative to the values of unipolar or bipolar hyphae set to 100%). (**D**) Relative chitinase activity mainly detecting chitinase Cts1 (Pohlmann et al., 2015) in yeast (left) or hyphal form (right, error bars, s.e.m.; n = 5 independent experiments).

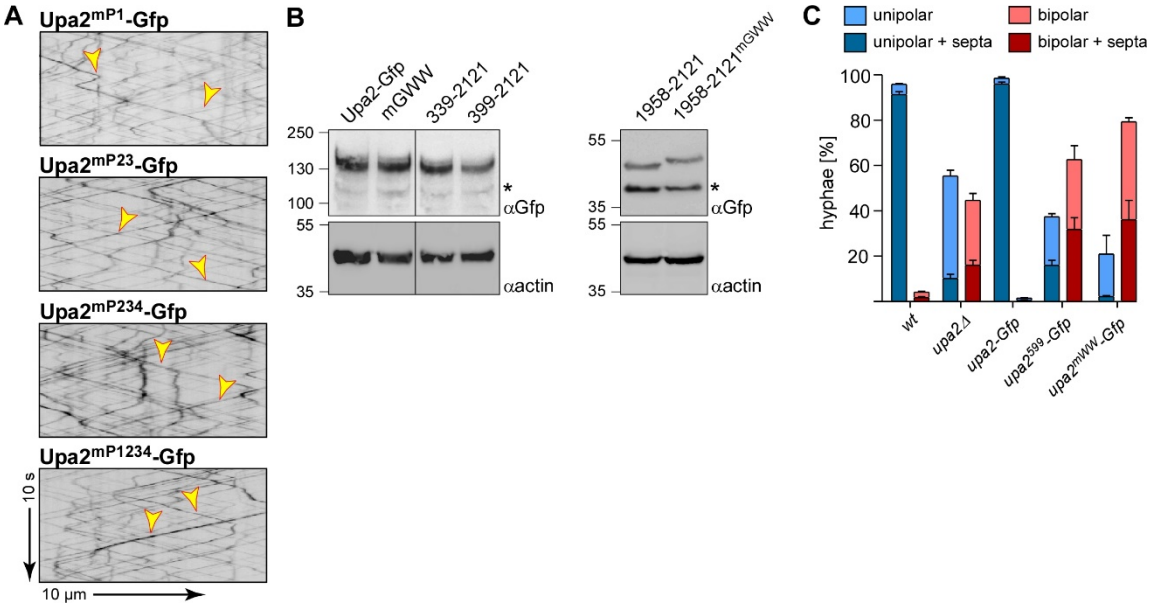

Supplementary Figure S3. The GWW motif of Upa2 is essential for correct hyphal growth.

(**A**) Kymographs of AB33 hyphae (6 h.p.i.) expressing versions of Upa2-Gfp with mutations in PAM2 motif as indicated (arrow length on the left and bottom indicate time and distance, respectively). Bidirectional movement is visible as diagonal lines (yellow arrowheads). (**B**) Western blot analysis demonstrating equal amounts of Upa2-Gfp versions using αGfp antibody (top panel). Expected molecular weight: Upa2-Gfp, 259 kDa; Upa2^{mGWW}-Gfp, 259 kDa; Upa2$^{339-2121}$-Gfp, 224 kDa; Upa2$^{399-2121}$-Gfp, 217 kDa; Upa2$^{1958-2121}$-Gfp, 46 kDa; Upa2$^{1958-2121mGWW}$-Gfp, 46 kDa. Note, that the molecular weight of Upa2-Gfp, Upa2^{mGWW}-Gfp, Upa2$^{339-2121}$-Gfp and Upa2$^{399-2121}$-Gfp appeared smaller in gel electrophoresis. Due to the change of two tryptophans to alanine, the running behaviour of Upa2$^{1958-2121mGWW}$-Gfp was different from Upa2$^{1958-2121}$-Gfp. Actin served as a loading control using αactin antibody (bottom panel; expected size for actin, 42 kDa). Asterisks in αGfp panels mark putative degradation products of Gfp-tagged Upa2. (**C**) Quantification of hyphal growth (6 h.p.i): unipolarity, bipolarity and septum formation were quantified (error bars, s.e.m.; n = 3 independent experiments, for each experiment >100 hyphae were counted per strain; note that septum formation is given relative to the values of unipolar or bipolar hyphae set to 100%).

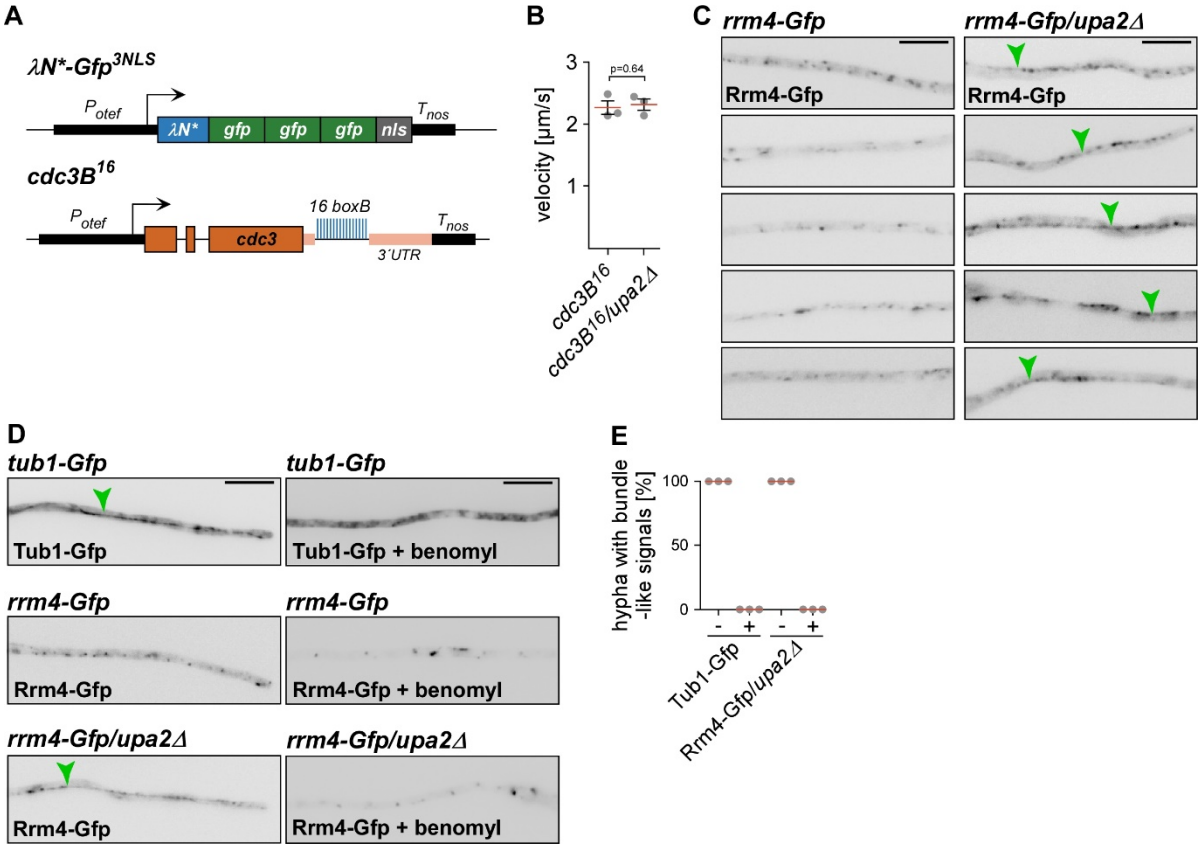

Supplementary Figure S4. Loss of Upa2 causes aberrant bundle-like accumulation of Rrm4-Gfp.

(**A**) Schematic representation of the λN* RNA live imaging system (P_{otef}, constitutively active promoter; T_{nos}, heterologous transcriptional terminator; cdc3, septin gene carrying 16 copies of the boxB hairpin in its 3′ UTR. λN*Gfp3 with nuclear localisation signal is recruited to mRNAs containing the λN*-binding sites designated boxB (Zander et al., 2016). (**B**) Velocity of fluorescent signals (velocity of tracks with > 5 µm processive movement; data points representing means from n = 3 independent experiments, with mean of means, red line, and s.e.m.; paired two-tailed Student´s t-test; for each experiment at least 10 hyphae were analysed per strain). (**C**) Micrographs (inverted fluorescence image; size bar, 10 µm of AB33 hyphae (6 h.p.i.) expressing Rrm4-Gfp (green arrowheads indicate bundle-like accumulation of Rrm4-Gfp). (**D**) Micrographs (inverted fluorescence image; size bar, 10 µm) of AB33 hyphae (6 h.p.i.) expressing Tub1-Gfp (ectopic expression of Tub1 fused N-terminally with Gfp, Steinberg & Fuchs, 2004) or Rrm4-Gfp (green arrowheads indicate bundle-like accumulation of Rrm4-Gfp). Hyphae on the right were treated with the microtubule inhibitor benomyl. (**E**) Quantification of bundle structures in strains expressing Gfp-Tub1 or Rrm4-Gfp with and without treatment of microtubule inhibitor benomyl (data points representing percentages from n = 3 independent experiments, with mean of means, red line; for each experiment at least 10 hyphae were analysed per strain).

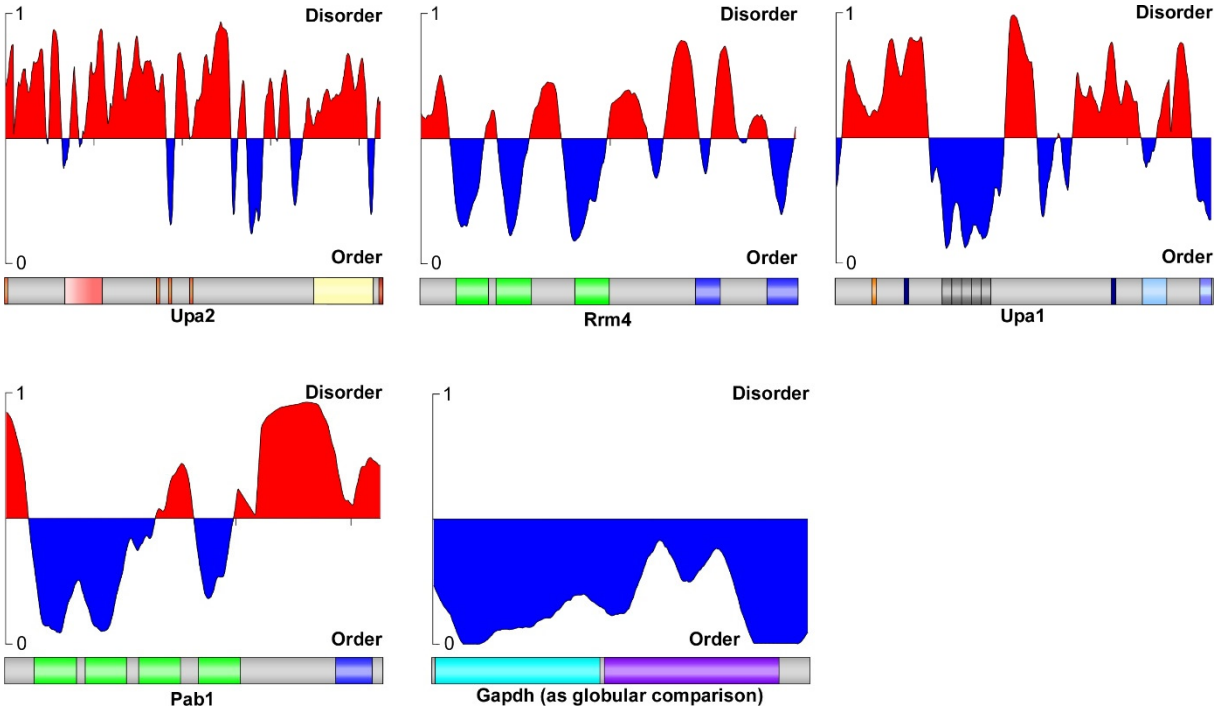

Supplementary Figure S5. Upa2 has extensive intrinsically disordered regions.

Analysis of intrinsically disordered regions using the PONDR algorithm VL3-BA. Amino acids are given prediction values between 0 and 1. Regions with values of 0.5 or above are considered disordered and are marked red, while peptide regions with values lower than 0.5 are considered ordered and are marked blue. The graphical output for the prediction is depicted in relation to the protein, shown below the graph. The size of the protein models is adjusted to the graph size. Extensive regions of Upa2 (>80%) are predicted to be disordered. Additionally, further known components of endosomal mRNA-transport, Rrm4, Upa1 and Pab1, show significant disordered stretches. Gapdh of *U. maydis* is shown as a structured protein in comparison.

838 **Supplementary Tables T1-T7**

839 **Supplementary Table T1: Description of *U. maydis* strains used in this study**

	Locus	Progenitor strain	Short description
AB33	*b*	FB2	*Pnar:bW2bE1*, expression of active b heterodimer under control of the *nar1* promoter, strain grows filamentously upon changing the nitrogen source.
AB33rrm4Δ	*rrm4*	AB33	carrying a deletion of *rrm4*.
AB33upa1Δ	*upa1*	AB33	carrying a deletion of *upa1*.
AB33upa2Δ	*upa2*	AB33	carrying a deletion of *upa2*.
AB33upa2-Gfp	*upa2*	AB33	expressing Upa2 C-terminally fused to eGfp.
AB33upa2^{mP1}-Gfp	*upa2*	AB33upa2Δ	expressing Upa2^{mP1} C-terminally fused to eGfp. Upa2^{mP1} carries the amino acid substitutions L6A, V8A and F13A in the first PAM2-motif.
AB33upa2^{mP234}-Gfp	*upa2*	AB33upa2Δ	expressing Upa2^{mP234} C-terminally fused to eGfp. Upa2^{mP234} carries the amino acid substitutions L863A and F870A in the second PAM2-motif, the amino acid substitutions L925A und F932A in the third PAM2-motif and L1051A und F1058A in the fourth PAM2-motif.
AB33upa2^{mP1234}-Gfp	*upa2*	AB33upa2Δ	expressing Upa2^{mP234} C-terminally fused to eGfp. Upa2^{mP1234} carries the amino acid substitutions L6A, V8A and F13A in the first PAM2-motif, L863A and F870A in the second PAM2-motif, L925A und F932A in the third PAM2-motif and L1051A und F1058A in the fourth PAM2-motif.
AB33rrm4-Gfp	*rrm4*	AB33rrm4Δ	expressing Rrm4 C-terminally fused to eGfp.
AB33pab1-Gfp	*pab1*	AB33	expressing Pab1 C-terminally fused to eGfp.
AB33upa2-Gfp/rrm4-mCherry	*upa2* *rrm4*	AB33upa2-Gfp	expressing Upa2 C-terminally fused to eGfp and Rrm4 C-terminally fused to mCherry,
AB33upa2-Gfp/pab1-mCherry	*upa2* *pab1*	AB33upa2-Gfp	expressing Upa2 C-terminally fused to eGfp and Pab1 C-terminally fused to mCherry,
AB33pab1-Gfp/rrm4Δ	*pab1* *rrm4*	AB33pab1-Gfp	expressing Pab1 C-terminally fused to eGfp and carrying a deletion of *rrm4*
AB33upa1-Gfp/rrm4Δ	*upa1* *rrm4*	AB33upa1-Gfp	expressing Upa1 C-terminally fused to eGfp and carrying a deletion of *rrm4*
AB33upa2-Gfp/rrm4Δ	*upa2* *rrm4*	AB33upa2-Gfp	expressing Upa2 C-terminally fused to eGfp and carrying a deletion of *rrm4*
AB33upa2-Gfp/rrm4^{mR1}-Rfp	*upa2* *rrm4*	AB33upa2-Gfp	expressing Upa2 C-terminally fused to eGfp and Rrm4 containing mutations in the first RRM C-terminally fused to mRFP. The conserved amino acids TVEF (aa 116-119) in the RNP2-motif of RRM1 were replaced by AAAA .
AB33pab1-Gfp/rrm4^{mR1}-Rfp	*pab1* *rrm4*	AB33pab1-Gfp	expressing Pab1 C-terminally fused to eGfp and Rrm4 containing mutations in the first RRM C-terminally fused to mRFP. The conserved amino acids TVEF (aa 116-119) in the RNP2-motif of RRM1 were replaced by AAAA .
AB33upa2$^{339-2121}$-Gfp	*upa2*	AB33upa2Δ	expressing Upa2$^{339–2121}$ C-terminally fused to eGfp. Like Upa2-Gfp, but carrying a N-terminal truncation from aa 1-338.
AB33upa2$^{399-2121}$-Gfp	*upa2*	AB33upa2Δ	expressing Upa2$^{399–2121}$ C-terminally fused to eGfp. Like Upa2-Gfp, but carrying a N-terminal truncation from aa 1-398.
AB33upa2$^{496-2121}$-Gfp	*upa2*	AB33upa2Δ	expressing Upa2$^{496–2121}$ C-terminally fused to eGfp. Like Upa2-Gfp, but carrying a N-terminal truncation from aa 1-495.
AB33upa2$^{599-2121}$-Gfp	*upa2*	AB33upa2Δ	expressing Upa2$^{599–2121}$ C-terminally fused to eGfp. Like Upa2-Gfp, but carrying a N-terminal truncation from aa 1-598.
AB33upa2$^{960-2121}$-Gfp	*upa2*	AB33upa2Δ	expressing Upa2$^{960–2121}$ C-terminally fused to eGfp. Like Upa2-Gfp, but carrying a N-terminal truncation from aa 1-959.
AB33upa2$^{1217-2121}$-Gfp	*upa2*	AB33upa2Δ	expressing Upa2$^{1217–2121}$ C-terminally fused to eGfp. Like Upa2-Gfp, but carrying a N-terminal truncation from aa 1-1216.

AB33upa2$^{1721-2121}$-Gfp	*upa2*	AB33upa2Δ	expressing Upa2$^{1712-2121}$ C-terminally fused to eGfp. Like Upa2-Gfp, but carrying a N-terminal truncation from aa 1-1720.
AB33upa2$^{1958-2121}$-Gfp	*upa2*	AB33upa2Δ	expressing Upa2$^{1958-2121}$ C-terminally fused to eGfp. Like Upa2-Gfp, but carrying a N-terminal truncation from aa 1-1957.
AB33upa2$^{1721-2070}$-Gfp	*upa2*	AB33upa2Δ	expressing Upa2$^{1721-2070}$ C-terminally fused to eGfp. Like Upa2-Gfp, but carrying a N-terminal truncation from aa 1-1720 and a C-terminal truncation from 2071-2121.
AB33upa2$^{1958-2121_mGWW}$-Gfp	*upa2*	AB33upa2Δ	expressing Upa2$^{1958-2121_mGWW}$ C-terminally fused to eGfp. Like Upa2$^{1958-2121}$-Gfp, but carrying the amino acid substitutions G2118A, W2019A and W2120A in the GWW-motif.
AB33upa2^{mGWW}-Gfp	*upa2*	AB33upa2Δ	expressing Upa2^{mGWW} C-terminally fused to eGfp. Like Upa2-Gfp, but carrying the amino acid substitutions G2118A, W2019A and W2120A in the GWW-motif.
AB33rrm4-Gfp/upa2Δ	*rrm4* *upa2*	AB33rrm4-Gfp	expressing Rrm4 C-terminally fused to eGfp and carrying a deletion of *upa2*.
AB33pab1-Gfp/upa2Δ	*pab1* *upa2*	AB33pab1-Gfp	expressing Pab1 C-terminally fused to eGfp and carrying a deletion of *upa2*.
AB33cdc3B^{16}/λN*^{NLS}-Gfp^{3}	*cdc3* *ip^{S}*	AB33cdc3B^{16}	expressing λN*-peptide fused to triple eGfp and *cdc3* mRNA tagged with 16 copies of boxB binding site.
AB33cdc3B^{16}/λN*^{NLS}-Gfp^{3}/upa2Δ	*cdc3* *ip^{S}* *upa2*	AB33cdc3B^{16}/λN*^{NLS}-Gfp^{3}	expressing and λN*-peptide fused to triple eGfp and *cdc3* mRNA tagged with 16 copies of boxB binding site. Additionally carrying a deletion of *upa2*.
AB33cdc3-Gfp	*cdc3*	AB33	expressing Cdc3 N-terminally fused to eGfp.
AB33cdc3-Gfp/upa2Δ	*cdc3* *upa2*	AB33cdc3-Gfp	expressing Cdc3 N-terminally fused to eGfp and carrying a deletion of *upa2*.
AB33tub1-Gfp	*tub1*	AB33	expressing Tub1 (alpha tubulin) N-terminally fused to eGfp. *Tub1-Gfp* is inserted ectopically in the *ip^{S}* locus and under the control of the constitutive *otef* promoter

840

841 **Supplementary Table T2: Generation of *U. maydis* strains used in this study**

Strains	Relevant genotype	Uma	Reference	Transformed plasmid	Locus	Progenitor
AB33	*a2* P_{nar}*:bW2 bE1*	133	Brachmann, 2001	pAB33	*b*	FB2
AB33rrm4Δ	*rrm4Δ*	273	Becht, 2006	pRrm4Δ_HygR (pUMa495)	*rrm4*	AB33
AB33upa1Δ	*upa1Δ*	859	Pohlmann, 2015	pUpa1Δ_HygR (pUMa1574)	*upa1*	AB33
AB33upa2Δ	*upa2Δ*	1505	this study	pUpa2Δ_NatR (pUMa2408)	*upa2*	AB33upa2Δ_HygR
AB33upa2-Gfp	*upa2-Gfp*	1791	this study	pUpa2-Gfp _HygR (pUMa2654)	*upa2*	AB33upa2Δ
AB33upa2^{mP1}-Gfp	*upa2^{mP1}-Gfp*	2373	this study	pUpa1^{mP1}-Gfp _NatR (pUMa3422)	*upa2*	AB33upa2Δ
AB33upa2^{mP234}-Gfp	*upa2^{mP234}-Gfp*	2375	this study	pUpa1^{mP234}-Gfp _NatR (pUMa3424)	*upa2*	AB33upa2Δ
AB33upa2^{mP1234}-Gfp	*upa2^{mP1234}-Gfp*	2376	this study	pUpa1^{mP1234}-Gfp _NatR (pUMa3426)	*upa2*	AB33upa2Δ
AB33rrm4-Gfp	*rrm4-Gfp*	274	Becht, 2006	pRrm4-Gfp_NatR (pUMa496)	*rrm4*	AB33rrm4Δ
AB33pab1-Gfp	*pab1-Gfp*	389	König, 2009	pPab1-Gfp_NatR (pUMa805)	*pab1*	AB33
AB33upa2-Gfp/rrm4-mCherry	*rrm4-mCherry*	2132	this study	pRrm4-mCherry _NatR (pUMa2964)	*rrm4*	AB33upa2-Gfp
AB33upa2-Gfp/pab1-mCherry	*rab1-mCherry*	2131	this study	pPab1-mCherry _NatR (pUMa2963)	*pab1*	AB33upa2-Gfp
AB33pab1-Gfp/rrm4Δ	*rrm4Δ*	472	König, 2009	pRrm4Δ_HygR (pUMa495)	*rrm4*	AB33pab1-Gfp
AB33upa1-Gfp/rrm4Δ	*rrm4Δ*	1048	Pohlmann, 2015	pRrm4Δ2_HygR (pUMa1391)	*rrm4*	AB33upa1-Gfp
AB33upa2-Gfp/rrm4Δ	*rrm4Δ*	515	this study	pRrm4Δ_HygR (pUMa495)	*rrm4*	AB33upa2-Gfp
AB33upa2-Gfp/rrm4^{mR1}-Rfp	*upa2-Gfp rrm4^{mR1}-Rfp*	896	this study	pRrm4^{mR1}-Rfp_HygR (pUMa1006)	*rrm4*	AB33upa2-Gfp
AB33pab1-Gfp/rrm4^{mR1}-Rfp	*pab1-Gfp rrm4^{mR1}-Rfp*	758	Baumann, 2014	pRrm4^{mR1}-Rfp_HygR (pUMa1006)	*rrm4*	AB33pab1-Gfp
AB33upa2$^{339-2121}$-Gfp	*upa2$^{339-2121}$-Gfp*	2715	this study	pUpa2$^{339-2121}$-Gfp _HygR (pUMa3897)	*upa2*	AB33upa2Δ
AB33upa2$^{399-2121}$-Gfp	*upa2$^{399-2121}$-Gfp*	2613	this study	pUpa2$^{399-2121}$-Gfp _HygR (pUMa3719)	*upa2*	AB33upa2Δ
AB33upa2$^{496-2121}$-Gfp	*upa2$^{496-2121}$-Gfp*	2615	this study	pUpa2$^{496-2121}$-Gfp _HygR (pUMa3720)	*upa2*	AB33upa2Δ

AB33upa2$^{599-2121}$-Gfp	*upa2$^{599-2121}$-Gfp*	1789	this study	pUpa2$^{599-2121}$-Gfp _HygR (pUMa2652)	*upa2*	AB33upa2Δ
AB33upa2$^{960-2121}$-Gfp	*upa2$^{960-2121}$-Gfp*	1788	this study	pUpa2$^{960-2121}$-Gfp _HygR (pUMa2651)	*upa2*	AB33upa2Δ
AB33upa2$^{1217-2121}$-Gfp	*upa2$^{1217-2121}$-Gfp*	1787	this study	pUpa2$^{1217-2121}$-Gfp _HygR (pUMa2650)	*upa2*	AB33upa2Δ
AB33upa2$^{1721-2121}$-Gfp	*upa2$^{1721-2121}$-Gfp*	1493	this study	pUpa2$^{1721-2121}$-Gfp _HygR (pUMa2394)	*upa2*	AB33upa2Δ
AB33upa2$^{1958-2121}$-Gfp	*upa2$^{1958-2121}$-Gfp*	1763	this study	pUpa2$^{1958-2121}$-Gfp _HygR (pUMa2721)	*upa2*	AB33upa2Δ
AB33upa2$^{1721-2070}$-Gfp	*upa2$^{1721-2070}$-Gfp*	1476	this study	pUpa2$^{1721-2070}$-Gfp _HygR (pUMa2432)	*upa2*	AB33upa2Δ
AB33upa2$^{1958-2121_mGWW}$-Gfp	*upa2$^{1958-2121_mGWW1}$_Gfp*	2176	this study	pUpa2$^{1958-2121_mGWW}$-Gfp _HygR (pUMa3180)	*upa2*	AB33upa2Δ
AB33upa2^{mGWW}-Gfp	*upa2^{mGWW}-Gfp*	1893	this study	pUpa2^{mGWW}-Gfp _HygR (pUMa2862)	*upa2*	AB33upa2Δ
AB33rrm4-Gfp/upa2Δ	*rrm4-Gfp upa2Δ*	1164	this study	pUpa2Δ_HygR (pUMa691)	*upa2*	AB33rrm4-Gfp
AB33pab1-Gfp/upa2Δ	*pab1-Gfp upa2Δ*	1165	this study	pUpa2Δ_HygR (pUMa691)	*upa2*	AB33pab1-Gfp
AB33cdc3B^{16}/λN*^{NLS}-Gfp^{3}	*cdc3B^{16} λN*^{NLS}-Gfp^{3}*	874	this study	pP$_{otef}$λN*^{3NLS}-Gfp _CbxR (pUMa1572)	*ip^{S}*	AB33cdc3B^{16}
AB33cdc3B^{16}/λN*^{NLS}-Gfp^{3} /upa2Δ	*cdc3B^{16} λN*^{NLS}-Gfp^{3} upa2Δ*	2099	this study	pUpa2Δ_HygR (pUMa691)	*upa1*	AB33cdc3B^{16} /λN*^{NLS}-Gfp^{3}
AB33cdc3-Gfp	*cdc3-Gfp*	449	Baumann, 2014	pCdc3-Gfp^{N}_NatR (pUMa1028)	*cdc3*	AB33
AB33cdc3-Gfp/upa2Δ	*cdc3-Gfp upa2Δ*	941	this study	pUpa2Δ_HygR (pUMa691)	*upa1*	AB33cdc3-Gfp
AB33tub1-Gfp	*tub1-Gfp*	498	This study	pTub1-Gfp_CbxR (pUMa508)	*tub1*	AB33

842

843 **Supplementary Table T3: Description of plasmids used for *U. maydis* strain generation**

Plasmid	pUMa	Resistance cassette	Short description
pAB33	705	SfiI-insert of pMF2-2p	Published (Brachmann, 2001)
pRrm4Δ_HygR	495	SfiI-insert of pMF1hs	Published (Becht, 2006)
pUpa1Δ_HygR	1574	SfiI-insert of pMF1hs	Published (Pohlmann, 2015)
pUpa2Δ_NatR	2408	SfiI-insert of pMF1n	Plasmid for generating deletion mutants of *upa2*. Resistance cassette is flanked by 2 kb upstream and 1.4 kb downstream region of *upa2*. Flanking regions were amplified by PCR using oMF939/oMF940 and oMF941/oMF942 and UM521 wild-type DNA as template.
pUpa2-Gfp _HygR	2654	SfiI-insert of pMF5-1n (with removed NdeI)	Plasmid for generating eGfp fusions of *upa2*. A cassette containing Gfp, the T_{nos} terminator and a hygromycin resistance cassette is flanked by 7.5 kb upstream region including 6.5 kb of the *upa1* ORF and 1.2 kb downstream region of *upa1*. Flanking regions were amplified by PCR using oDD160/oDD161 and oDD162/oDD163 and UM521 wild-type DNA as template.
pUpa2^{mP1}-Gfp _NatR	3422	SfiI-insert of pMF5-1n (with removed NdeI)	Plasmid for generating eGfp fusions of *upa2^{mP1}*. Like pUpa2-Gfp_NatR, but carrying the amino acid substitutions L6A, V8A and F13A in the first PAM2-motif.
pUpa2^{mP234}-Gfp _NatR	3424	SfiI-insert of pMF5-1n (with removed NdeI)	Plasmid for generating eGfp fusions of *upa2^{mP234}*. Like pUpa2-Gfp_NatR, but carrying the amino acid substitutions L863A and F870A in the second PAM2-motif, the amino acid substitutions L925A und F932A in the third PAM2-motif and L1051A und F1058A in the fourth PAM2-motif.
pUpa2^{mP1234}-Gfp _NatR	3426	SfiI-insert of pMF5-1n (with removed NdeI)	Plasmid for generating eGfp fusions of *upa2^{mP1234}*. Like pUpa2-Gfp_NatR, but carrying the amino acid substitutions L6A, V8A and F13A in the first PAM2-motif, the amino acid substitutions L863A and F870A in the second PAM2-motif, the amino acid substitutions L925A und F932A in the third PAM2-motif and L1051A und F1058A in the fourth PAM2-motif.
pRrm4-Gfp_NatR	496	SfiI-insert of pMF5-1n	Published (Becht, 2006).
pPab1-Gfp_NatR	805	SfiI-insert of pMF5-1n	Published (König, 2009).
pRrm4-mCherry _NatR	2964	SfiI-insert of pMF5-5n	Plasmid for generating mCherry fusions of *rrm4*. Like pRrm4-Gfp_NatR, but the C-terminal Gfp-tag was exchanged with an mCherry-tag.
pPab1-mCherry _NatR	2963	SfiI-insert of pMF5-5n	Plasmid for generating mCherry fusions of *pab1*. Like pPab1-Gfp_NatR, but the C-terminal Gfp-tag was exchanged with an mCherry-tag.
pRrm4Δ2_HygR	1391	SfiI-insert of pMF1hl	Published (Pohlmann, 2015)
pRrm4^{mR1}-Rfp_HygR	1006	SfiI-insert of pMF5-2h	Published (Baumann, 2014)
pUpa2$^{284-2121}$-Gfp_HygR	2653	SfiI-insert of pMF5-1n (with removed NdeI)	Plasmid for generating eGfp fusions of *upa2$^{284-2121}$*. Like pUpa2-Gfp_NatR, but carrying a N-terminal truncation from aa 1-283.
pUpa2$^{339-2121}$-Gfp_HygR	3897	SfiI-insert of pMF5-1n (with removed NdeI)	Plasmid for generating eGfp fusions of *upa2$^{339-2121}$*. Like pUpa2-Gfp_NatR, but carrying a N-terminal truncation from aa 1-338.
pUpa2$^{399-2121}$-Gfp_HygR	3719	SfiI-insert of pMF5-1n (with removed NdeI)	Plasmid for generating eGfp fusions of *upa2$^{399-2121}$*. Like pUpa2-Gfp_NatR, but carrying a N-terminal truncation from aa 1-398.
pUpa2$^{496-2121}$-Gfp_HygR	3720	SfiI-insert of pMF5-1n (with removed NdeI)	Plasmid for generating eGfp fusions of *upa2$^{496-2121}$*. Like pUpa2-Gfp_NatR, but carrying a N-terminal truncation from aa 1-495.
pUpa2$^{599-2121}$-Gfp_HygR	2652	SfiI-insert of pMF5-1n (with removed NdeI)	Plasmid for generating eGfp fusions of *upa2$^{599-2121}$*. Like pUpa2-Gfp_NatR, but carrying a N-terminal truncation from aa 1-598.
pUpa2$^{960-2121}$-Gfp_HygR	2651	SfiI-insert of pMF5-1n (with removed NdeI)	Plasmid for generating eGfp fusions of *upa2$^{960-2121}$*. Like pUpa2-Gfp_NatR, but carrying a N-terminal truncation from aa 1-959.
pUpa2$^{1217-2121}$-Gfp_HygR	2650	SfiI-insert of pMF5-1n (with removed NdeI)	Plasmid for generating eGfp fusions of *upa2$^{1217-2121}$*. Like pUpa2-Gfp_NatR, but carrying a N-terminal truncation from aa 1-1216.
pUpa2$^{1721-2121}$-Gfp_HygR	2394	SfiI-insert of pMF5-1n (with removed NdeI)	Plasmid for generating eGfp fusions of *upa2$^{1721-2121}$*. Like pUpa2-Gfp_NatR, but carrying a N-terminal truncation from aa 1-1720.
pUpa2$^{1958-2121}$-Gfp_HygR	2721	SfiI-insert of pMF5-1n (with removed NdeI)	Plasmid for generating eGfp fusions of *upa2$^{1958-2121}$*. Like pUpa2-Gfp_NatR, but carrying a N-terminal truncation from aa 1-1957.

pUpa2$^{1721-2070}$-Gfp_HygR	2432	SfiI-insert of pMF5-1n (with removed NdeI)	Plasmid for generating eGfp fusions of *upa2$^{1721-2070}$*. Like pUpa2-Gfp_NatR, but carrying a N-terminal truncation from aa 1-1720 and a C-terminal truncation from 2071-2121.
pUpa2$^{1958-2121_mGWW}$-Gfp_HygR	3180	SfiI-insert of pMF5-1n (with removed NdeI)	Plasmid for generating eGfp fusions of *upa2$^{1958-2121_mGWW}$*. Like pUpa2$^{1958-2121}$-Gfp_NatR, but carrying the amino acid substitutions G2118A, W2019A and W2120A in the GWW-motif.
pUpa2^{mGWW}-Gfp_HygR	2862	SfiI-insert of pMF5-1n (with removed NdeI)	Plasmid for generating eGfp fusions of *upa2^{mGWW1}*. Like pUpa2-Gfp_NatR, but carrying the amino acid substitutions G2118A, W2019A and W2120A in the GWW-motif.
pUpa2Δ_HygR	691	SfiI-insert of pMF1hs	Plasmid for generating deletion mutants of *upa2*. Lie pUpa2Δ_NatR, but the Sfi-insert of pMF1n containing the nourseothricin resistance cassette has been replaced by the SfiI-insert of pMF1hs containing an hygromycin resistance cassette.
pP$_{otef}$λN*^{3NLS}-Gfp_CbxR	1572	CbxR for integration at *ip^{S}* locus	Published (Pohlmann, 2015).
pCdc3-Gfp^{N}_NatR	1028	SfiI-insert of pMF1n	Published (Baumann, 2014).
pTub1-Gfp_CbxR	508	CbxR for integration at *ip^{S}* locus	Plasmid for the extopic expression of Tub1 (alpha tubulin) N-terminally fused to eGfp. Tub1-Gfp is under control of the constitutive acitve *otef* promoter.

844

845 **Supplementary Table T4: Description of plasmids used for yeast two-hybrid analyses**

Plasmid	pUMa	Gene	Short description
pGADT7-DS	*1624*		Plasmid for the expression of hybrid proteins, N-terminally fused to a nuclear localisation signal (NLS) of the simian virus 40 (SV40), followed by the Gal4 activation domain (aa 768-881) and an HA-epitope for Western Blot detection. Resulting hybrid proteins are termed AD-"X". For positive selection of transformants on minimal medium this plasmid carries a *LEU2* auxotrophy marker. This plasmid contains two diverse SfiI-restriction sites for cloning purposes (Dualsystems Biotech, Schlieren, Switzerland).
pGBKT7-SfiI MCS	*1625*		Plasmid for the expression of hybrid proteins, N-terminally fused to the Gal4 DNA-binding domain (aa 1-147), followed by a c-Myc-epitope for Western Blot detection. Resulting hybrid proteins are termed BD-"X". For positive selection of transformants on minimal medium, this plasmid carries a *TRP1* auxotrophy marker. This plasmid contains two diverse SfiI-restriction sites for cloning purposes. (Clontech Laboratories, Inc., Mountain View, CA, USA).
pGADT7-T	*1636*		Plasmid for the expression of a N-terminal AD-fusion of the large T-antigen of SV40. It interacts with BD-p53 as a positive control (Clontech).
pGBKT7-p53	*1638*		Plasmid for the expression of a N-terminal BD-fusion of the murine p53. It interacts with AD-T as a positive control (Clontech).
pGBKT7-Lam	*1637*		Plasmid for the expression of a N-terminal BD-fusion with the human nuclear protein Lamin C, which shows no interaction with most proteins and serves as negative control (Clontech).
pGBKT7-Rrm4	*1628*	*rrm4*	Plasmid for the expression of BD-Rrm4.
pGBKT7-Pab1	*1632*	*pab1*	Plasmid for the expression of BD-Pab1.
pGADT7-Upa2	*1631*	*upa2*	Plasmid for the expression of AD-Upa2.
pGADT7_upa2_1-1216	*3562*	*upa2*	Plasmid for the expression of AD-Upa2_1-1216. Like AD-Upa2 but carrying a C-terminal truncation from aa 1217-2121.
pGADT7_upa2_1217-2121	*3437*	*upa2*	Plasmid for the expression of AD-Upa2_1-1216. Like AD-Upa2 but carrying a N-terminal truncation from aa 1-1216.
pGBKT7-Pab1^{mM}	*1998*	*pab1*	Plasmid for the expression of BD-Pab1^{mM}. Like BD-Pab1, but carrying the amino acid substitutions Y580A, V583A, K593A and I598A in the MLLE domain.
pGBKT7_onlyMLLEpab1	*2000*	*pab1*	Plasmid for the expression of BD- MLLE^{Pab1}. For this the last 86 aa of the *pab1* ORF including the MLLE domain were fused to Gal4-BD and Myc.
pGADT7_upa2_1-1216^{mP1}	*3563*	*upa2*	Plasmid for the expression of AD- Upa2_1-1216^{mP1}. Like AD-Upa2_1-1216, but carrying the amino acid substitutions L6A, V8A and F13A in the first PAM2-motif.
pGADT7_upa2_1-1216^{mP234}	*3564*	*upa2*	Plasmid for the expression of AD- Upa2_1-1216^{mP1}. Like AD-Upa2_1-1216, but carrying the amino acid substitutions L863A and F870A in the second PAM2-motif, the amino acid substitutions L925A und F932A in the third PAM2-motif and L1051A und F1058A in the fourth PAM2-motif.
pGADT7_upa2_1-1216^{mP1234}	*3565*	*upa2*	Plasmid for the expression of AD- Upa2_1-1216^{mP1}. Like AD-Upa2_1-1216, but carrying the amino acid substitutions L6A, V8A and F13A in the first PAM2-motif, L863A and F870A in the second PAM2-motif, L925A und F932A in the third PAM2-motif and L1051A und F1058A in the fourth PAM2-motif.
pGBKT7-mMLLE^{pab1}	*3420*	*pab1*	Plasmid for the expression of BD- mMLLE^{Pab1}.Like BD-mMLLE^{Pab}, but carrying the amino acid substitutions Y580A, V583A, K593A and I598A in the MLLE domain.
pGADT7-upa1_1-194	*2002*	*upa1*	Plasmid for the expression of AD-Upa1_1-194. Expresses Upa1 as BD-fusion, but carrying a C-terminal truncation from aa 195-1287.
pGADT7_upa2_1721-2121	*3313*	*upa2*	Plasmid for the expression of AD-Upa2_1721-2121. Like AD-Upa2 but carrying a N-terminal truncation from aa 1-1720.
pGBKT7_upa2_1721-2121	*3380*	*upa2*	Plasmid for the expression of BD-Upa2_1721-2121. Like AD-Upa2_1712-2121 but fused to BD.
pGADT7_upa2_1721-2121^{mGWW}	*3392*	*upa2*	Plasmid for the expression of AD-Upa2_1721-2121^{mGWW}. Like AD-Upa2_1712-2121, but carrying a triple amino acid exchange of the conserved GWW to AAA (aa 2118-2120)

846

847 **Supplementary Table T5: Description of plasmids used for pulldown experiments**

Plasmid	pUMa	Short description
pGEX_GST	1881	Plasmid for the expression of the GST (Glutathione S transferase)-tag alone. Expression is regulated by tac promoter. The plasmid also contains a *lacI*^{q} gene for use in *E. coli*. The plasmid carries an ampicillin resistance for selection. This vector is based on pGEX-2T (GE Healthcare).
pGEX_GST-MLLE^{Pab1}	2187	Plasmid for the expression of the GST-MLLE^{Pab1}. The last 86 aa of the *pab1* ORF including the MLLE domain were N-terminally fused to a GST-tag.
pGEX_GST-Rrm4$^{720-792}$	2385	Plasmid for the expression of the GST-Rrm4$^{720-792}$. A region of Rrm4 comprising of amino acid 720-792 was N-terminally fused to a GST-tag.
pET15B_Upa2_834-1216	3468	Plasmid for the expression of a His$_6$_ Upa2_834-1216 in *E. coli*. Upa2 (aa 834-1216) which includes the coding regions for the PAM2 motifs 2, 3, 4 was N-terminally fused to a 6x histidine-tag. Expression is regulated by lacO. The plasmid carries an ampicillin resistance for selection.
pET15B_Upa2_834-1216^{mP23}	3469	Plasmid for the expression of a His$_6$_ Upa2_834-1216^{mP23} in *E. coli*. Like Upa2_834-1216, but carrying the amino acid substitutions L863A and F870A in the second PAM2 motif, the amino acid substitutions L925A und F932A in the third PAM2 motif. Expression is regulated by lacO. The plasmid carries an ampicillin resistance for selection.
pET15B_Upa2_834-1216^{mP234}	3470	Plasmid for the expression of a His$_6$_ Upa2_834-1216^{mP234} in *E. coli*. Like Upa2_834-1216, but carrying the amino acid substitutions L863A and F870A in the second PAM2 motif, the amino acid substitutions L925A und F932A in the third PAM2 motif and L1051A und F1058A in the fourth PAM2 motif. Expression is regulated by lacO. The plasmid carries an ampicillin resistance for selection.

848

849 **Supplementary Table T6: DNA oligonucleotides used in this study**

Designation	Nucleotide sequence (5' --> 3')	Remarks
oMF938	CTCGCGTTTCCACTTGCC	*upa2* u1 (deletion)
oMF939	GCTGAGTTGACGTTGGGC	*upa2* u2 (deletion)
oMF940	TTCGGCCATCTAGGCCTTGAGACTGCTGCCCTCC	*upa2* u3 (deletion)
oMF941	TGAGGCCTGAGTGGCCTCGAGGTGGATGAAGGCG	*upa2* d1 (deletion)
oMF942	AAGCAGCGAGTCGTACGC	*upa2* d2 (deletion)
oMF943	GCCTGTTGTCGTTGAGCC	*upa2* d3 (deletion)
oMF944	CACCAGCACCTAGTCAGC	*upa2* p1 (deletion)
oMF945	TGAATCATACCGCCCGGC	*upa2* p2 (deletion)
oDD144	GGTCTCGGATCGCATATGGATGCTCTGCACAGGAGGCTCG	*upa2* ORF 1721 fwd
oDD145	GGTCTCCTGGCGCGTCTTTTGCTTTTCGACCG	*upa2* ORF 2070 rev
oDD160	GGTCTCGCCTGCAATATTTGTAGTCAACTGCCTCTTTG	*upa2* u2 (fusion)
oDD161	GGTCTCGGATCCTTGATGAGCTAGACAGGAAAC	*upa2* u3 (fusion)
oDD162	GGTCTCCGGCCAGTGGTAATGATTCGAATGCC	*upa2* d1 (fusion)
oDD163	GGTCTCCCTGCAATATTCTCGGTATGCGTTAGAATG	*upa2* d2 (fusion)
oDD526	GGTCTCCTGGCAGACCACCACCCGCCTTC	*upa2* ORF 2121 rev
oDD578	ATAACATATGTGGGGCGATCGCCGCACG	*upa2* 1217-1414
oDD579	CGTGCGGCGATCGCCCCATCG	*upa2* 960-1216
oDD580	CTTGACCTGCCTCAGCGCGTG	*upa2* 1415-1711
oDD581	ATAACATATGAATGCGGCGCCCAACGGG	*upa2* 599-959
oDD582	CGTTGGGCGCCGCATTCGGAC	*upa2* 284-598
oDD583	GTGCCATATGGAGGGCAGCAGTC	*upa2* 1-283
oDD584	CGCGCATATGCGTGCTAGCGAACCAGGTTC	*upa2* 284-598
oDD585	GAACCTGGTTCGCTAGCACGTG	*upa2* 1-283
oDD586	ATAACATATGGGGGCCGCGGTCAAGCCGAAT	*upa2* 1415-1711
oDD587	CATTCGGCTTGACCGCGGCCC	*upa2* 1217-1414
oDD588	CGCGCATATGGTAACTAGTGCTGATGGTGGTG	*upa2* 960-1216
oDD589	GCACCACCATCAGCACTAGTTACTGCGATGC	*upa2* 599-959

oDD604	GGTCTCGGATCCATATGAAGGCTGAAGAGCTCGCCGAAG	*upa2* 1958-2121
oDD741	GGTCTCGGATCCATATGGCTGCCGCGGCGGCCGCCGCGGCGCGTGTTCACATCGAGGATGT	mutGWW 1958
oRL422	AGAGGTTACATGGCCAAG	Y2H of *upa2*
oRL591	TGAGGCCATTACGGCCCATATGGAGGGCAGCAGTCTC	Y2H of *upa2*
oRL592	CGTGGCCGAGGCGGCCGTCAAGACCACCACCCGCCTTC	Y2H of *upa2*
oMB43	GGTCTCGCCTGGCTGAGGCAGGTCAAGCTGAAGCCGAG	*upa2* 1712-2121
oMB44	GGGTCTCGCGGCGCCTTCATCCACCTCGACCTCCTT	mutGWW
oMB45	GGTCTCGGCCGCCGCTTCTGCCAACGCGGCCACCATGGTG	mutGWW
oMB46	GGTCTCGCTGCGGCGCGCCGGCCGCTTTACTTGTACA	mutGWW
oMB922	GGTCTCAGCATCTATGCTCCGGTTTCGACGCC	Y2H 283 rev
oMB923	GGTCTCCGGCCAATGCGGCGCCCAACGGG	Y2H 599 fwd
oMB926	GGTCTCAGCATCTAAGACCACCACCCGCCTTC	Y2H 1721-2121
oMB958	GGTCTCCGGCCATGGAGGGCAGCAGTGCCAACGCCGCGGCGCCTGTGGCTAAGCCCAGCGGCG CTGCAAAC	mutPAM2-1
oMB959	GGTCTCCGGCCGATGCTCTGCACAGGAGG	Y2H 1721-2121
oMB970	GGTCTCCAGCGTCAGGATTGGCCAGCGAGATTCCAGAAGCTC	mutPAM2-2rev
oMB971	GGTCTCCCGCTAAGGAGGCCAAGTTCGGCGGGACAAGCGC	mutPAM2-2fwd
oMB972	GGTCTCCCGCACCCACATTGGCGTGAGCTGCATTCGTGGG	mutPAM2-3rev
oMB973	GGTCTCCTGCGGCTCCGGCCACCCCGGGCTTGTTTACCTTC	mutPAM2-3fwd
oMB974	GGTCTCCGGCATCAGCTGTCGCGCGGGATTCGTGTGAGAC	mutPAM2-4rev
oMB975	GGTCTCCTGCCCCATCGGCCGTGCCAACTTGGGCAAAAAG	mutPAM2-4fwd
oMB979	GGTCTCAGCATCTATCGAATGGATGGGACGTGTC	Y2H 1216 rev
oUP276	GGTCTCAGCATCTAAGAAGCGGCGGCGCCTTC	Y2H 1721 mutGWW
oUP327	TCGCATATGGAGGGCAGCAGTGCCAAC	mutGWW

850

851 **Supplementary Table T7: Accession numbers of phylogenetic analysis**

Organism	Rrm4 ortholog	Upa2 ortholog	Upa1 ortholog
Ustilago maydis	XP_011389820.1	XP_011391917.1	XP_011388912.1
Ustilago hordei	CCF52027.1	CCF50315.1	CCF52210.1
Ustilago bromivora	SAM82601.1	SAM85987.1	SAM82942.1
Sporisorium reilianum	CBQ73718.1	CBQ69926.1	CBQ72642.1
Sporisorium scitamineum	CDW98458.1	CDU22493.1	CDW96316.1
Moesziomyces antarcticus	XP_014657015.1	XP_014654742.1	XP_014656570.1
Melanopsichium pennsylvanicum	CDI54139.1	CDI55987.1	CDI53177.1
*Thecaphora thlaspeos**	THTG_06061	THTG_03355	THTG_01672
Malassezia globosa	n.a.	n.a.	XP_001732453.1**
Cryptococcus neoformans	XP_024512316.1***	n.a.	XP_569116.1***
Armillaria ostoyae	SJK98691.1	SJL05310.1	SJL02266.1
Coprinopsis cinerea	XP_001832566.2	XP_001828502.2	XP_001837291.2
Punctularia strigosozonata	XP_007384300.1	XP_007378248.1	XP_007382070.1
Serendipita indica	CCA67340.1	CCA73898.1	CCA71703.1 / CCA71704.1
Trametes versicolor	XP_008042363.1	XP_008033367.1	XP_008035292.1
Phanerochaete carnosa	XP_007393387.1	XP_007389854.1	XP_007391955.1

852 * *T. thlaspeos* specific gene descriptions were used, because the genome has not been published so far.
853 ** *M. globosa* Upa1 ortholog resembles the Pib1-like type of FYVE-proteins
854 *** *C. neoformans* proteins show weak or partial homology to Rrm4 and Upa1, and are considered not
855 functional, although their functionality was so far not assessed.

856 **Legends to Supplementary Videos**

857 **Supplementary Video V1**

858 Composite video showing Upa2-Gfp in comparison with other components of endosomal
859 transport mRNPs. (1st line) Upa2-Gfp is moving bidirectionally in hyphae. (2nd line) Upa2-Gfp
860 movement is abolished by treatment with microtubule inhibitor benomyl. (3rd line) Rrm4-Gfp
861 is moving bidirectionally in hyphae. (4th line) Pab1-Gfp is moving bidirectionally in hyphae.
862 Additionally, Pab1-Gfp shows a prominent localisation in the cytoplasm (size bar, 10 µm;
863 timescale in seconds, 150 ms exposure time, 150 frames, 6 frames/s display rate; MP4 format,
864 2373 kb; corresponds to Figure 3A).

865

866 **Supplementary Video V2**

867 Composite video showing co-localisation of Upa2-Gfp and Rrm4-mCherry (upper and lower
868 part, respectively). Both proteins co-localise in shuttling units in hyphae. Videos were recorded
869 simultaneously using dual-colour detection (size bar, 10 µm; timescale in seconds, 150 ms
870 exposure time, 150 frames, 6 frames/s display rate; MP4 format, 2387 kb; corresponds to Figure
871 3D).

872

873 **Supplementary Video V3**

874 Composite video showing movement of Upa1-Gfp in hyphae with or without Rrm4 (top and
875 bottom, respectively). Upa1-Gfp is moving bidirectionally in hyphae. Loss of Rrm4 results in
876 bipolar growing cell, but does not affect Upa1-Gfp shuttling (size bar, 10 µm, timescale in
877 seconds, 150 ms exposure time, 150 frames, 6 frames/s display rate; MP4 format, 2371 kb;
878 corresponds to Figure 4A, top).

879

880 **Supplementary Video V4**

881 Composite video showing movement of Pab1-Gfp in hyphae with and without Rrm4 (upper
882 and lower part, respectively). Pab1-Gfp is moving bidirectionally in the hyphal cell and shows
883 a prominent cytoplasmic localization. Loss of Rrm4 results in bipolar growing cell, and
884 abolishes Pab1-Gfp shuttling (size bar,10 µm; timescale in seconds, 150 ms exposure time, 150
885 frames, 6 frames/s display rate; MP4 format, 506 kb corresponds to Figure 4A center).

886 **Supplementary Video V5**

887 Composite video showing movement of Upa2-Gfp in hyphae with and without Rrm4 (upper
888 and lower part, respectively). Upa2-Gfp is moving bidirectionally in hyphae. Loss of Rrm4
889 results in bipolar growing cells, and abolishes Upa2-Gfp shuttling (size bar, 10 µm; timescale
890 in seconds, 150 ms exposure time, 150 frames, 6 frames/s display rate; MP4 format, 2364 kb
891 corresponds to Figure 4A, bottom).

892

893 **Supplementary Video V6**

894 Composite video showing co-localisation of Upa2-Gfp and Rrm4^{mR1}-mRfp (upper and lower
895 part, respectively) in hyphae. While Rrm4^{mR1}-Rfp is present in bidirectionally moving units,
896 Upa2-Gfp does not show processive movement. Videos were recorded simultaneously using
897 dual-colour detection (size bar, 10 µm; timescale in seconds, 150 ms exposure time, 150 frames,
898 6 frames/s display rate; MP4 format, 2300 kb; corresponds to Figure 4C, left).

899

900 **Supplementary Video V7**

901 Composite video showing co-localisation of Pab1-Gfp and Rrm4^{mR1}-mRfp (upper and lower
902 part, respectively) in hyphae. Rrm4^{mR1}-Rfp is present in bidirectionally moving units. Pab1-
903 Gfp shows strongly reduced shuttling. Videos were recorded simultaneously using dual-colour
904 detection (size bar, 10 µm; timescale in seconds, 150 ms exposure time, 150 frames, 6 frames/s
905 display rate; MP4 format, 2364 kb; corresponds to Figure 4C right).

906

907 **Supplementary Video V8**

908 Composite video showing movement of Upa2-Gfp and Upa2^{mGWW}-Gfp in hyphae (upper and
909 lower part, respectively). While Upa2-Gfp is moving bidirectionally, Upa2^{mGWW}-Gfp shuttling
910 is no longer detectable (size bar, 10 µm; timescale in seconds, 150 ms exposure time, 150
911 frames, 6 frames/s display rate; MP4 format, 2367 kb; corresponds to Figure 5H).

912

913 **Supplementary Video V9**

914 Composite video showing movement of Cdc3-Gfp with and without Upa2 in hyphae (upper
915 and lower part, respectively). While Upa2 is present, Cdc3-Gfp is moving bidirectionally and
916 forms a gradient starting from the hyphal tip, loss of Upa2 results in absence of Cdc3-Gfp
917 movement as well as gradient formation (size bar, 10 µm, timescale in seconds, 150 ms
918 exposure time, 150 frames, 6 frames/s display rate; MP4 format, 2247 kb; corresponds to Figure
919 6A).

920

921 **Supplementary Video V10**

922 Composite video showing movement of Pab1-Gfp with and without Upa2 in hyphae (upper and
923 lower part, respectively). While Pab1-Gfp is moving bidirectionally in the presence of Upa2,
924 loss of Upa2 results in reduced movement of Pab1-Gfp (size bar,10 µm; timescale in seconds,
925 150 ms exposure time, 150 frames, 6 frames/s display rate; MP4 format, 945 kb; corresponds
926 to Figure 6G).

927

928 **Supplementary Video V11**

929 Composite video showing movement of Rab5a-Gfp with and without Upa2 in hyphae (upper
930 and lower part, respectively). While Rab5a-Gfp is moving bidirectionally in the presence of

931 Upa2, loss of Upa2 results in bipolar growing cells, but does not drastically affect movement
932 of Rab5a-Gfp (size bar, 10 µm; timescale in seconds, 150 ms exposure time, 150 frames, 6
933 frames/s display rate; MP4 format; 1429 kb, corresponds to Figure 6G).
934

935 **Supplementary Video V12**
936 Composite video showing movement of Rrm4-Gfp with and without Upa2 in hyphae (upper
937 and lower part, respectively). While Rrm4-Gfp is moving bidirectionally in the presence of
938 Upa2, loss of Upa2 results in bipolar growing cells, but does not drastically affect movement
939 of Rrm4-Gfp. Note, the aberrant staining of a microtubule bundle (size bar, 10 µm, timescale
940 in seconds, 150 ms exposure time, 150 frames, 6 frames/s display rate; MP4 format; 948 kb
941 corresponds to Figure 6G).
942

943 **Supplementary Video V13**
944 Composite video showing movement of Upa1-Gfp with and without Upa2 in hyphae (upper
945 and lower part, respectively). While Upa1-Gfp is moving bidirectionally in the presence of
946 Upa2, loss of Upa2 results in bipolar growing cells, but does not drastically affect movement
947 of Upa1-Gfp (size bar, 10 µm; timescale in seconds, 150 ms exposure time, 150 frames, 6
948 frames/s display rate; MP4 format; 2357 kb corresponds to Figure 6G).